3D printing of biocompatible low molecular weight gels: Imbricated structures with sacrificial and persistent N-alkyl-d-galactonamides

Faniry Andriamiseza, Delphine Bordignon, Bruno Payré, Laurence Vaysse, Juliette Fitremann

F. Andriamiseza, D. Bordignon, B. Payré, L. Vaysse, J. Fitremann, 3D printing of biocompatible low molecular weight gels: Imbricated structures with sacrificial and persistent N-alkyl-d-galactonamides, Journal of Colloid and Interface Science. 617 (2022) 156–170.
https://doi.org/10.1016/j.jcis.2022.02.076.

3D printing of biocompatible low molecular weight gels: imbricated structures with sacrificial and persistent N-alkyl-D-galactonamides

Faniry Andriamiseza [a], Delphine Bordignon [a], Bruno Payré [b], Laurence Vaysse[c], Juliette Fitremann [a] *

Graphical Abstract

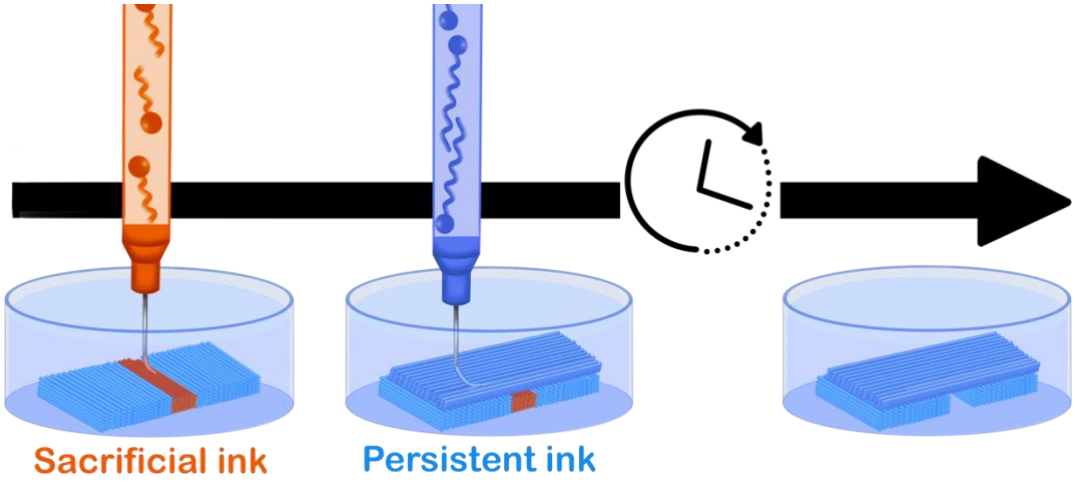

3D printing of biocompatible low molecular weight gels: imbricated structures with sacrificial and persistent N-alkyl-D-galactonamides

Faniry Andriamiseza [a], Delphine Bordignon [a], Bruno Payré [b], Laurence Vaysse[c], Juliette Fitremann [a] *

[a] Laboratoire des IMRCP, Université de Toulouse, CNRS UMR 5623, Université Toulouse III - Paul Sabatier, France

[b] Centre de Microscopie Electronique Appliquée à la Biologie (CMEAB), Faculté de Médecine Rangueil, Université de Toulouse III Paul Sabatier, Bâtiment A5, R.D.C., 133 Route de Narbonne, 31400 Toulouse, France

[c] RESTORE Research Center, Université de Toulouse, INSERM 1301, CNRS 5070, EFS, ENVT, Toulouse, France

Corresponding author:

Juliette Fitremann
Laboratoire des IMRCP
Bâtiment 2R1, Université Paul Sabatier Toulouse III
118 Route de Narbonne
31062 Toulouse cedex 9, France

Tel +33 5 61 55 68 04

juliette.fitremann@cnrs.fr

Other authors' emails

Faniry Andriamiseza	faniry-meva.andriamiseza@univ-tlse3.fr
Delphine Bordignon	bordignon@chimie.ups-tlse.fr
Bruno Payré	bruno.payre@univ-tlse3.fr
Laurence Vaysse	laurence.vaysse@inserm.fr

Abstract

Hypothesis: We have shown earlier that low molecular weight gels based on N-heptyl-D-galactonamide hydrogels can be 3D printed by solvent exchange, but they tend to dissolve in the printing bath. We wanted to explore the printing of less soluble N-alkyl-D-galactonamides with longer alkyl chains. Less soluble hydrogels could be good candidates as cell culture scaffolds.
Experiments: N-hexyl, N-octyl and N-nonyl-D-galactonamide solutions in dimethylsulfoxide are injected in a bath of water following patterns driven by a 2D drawing robot coupled to a z-platform. Solubilization of the gels with time has been determined and solubility of the gelators has been measured by NMR. Imbricated structures have been built with N-nonyl-D-galactonamide as a persistent ink and N-hexyl or N-heptyl-D-galactonamide as sacrificial inks. Human mesenchymal stem cells have been cultured on N-nonyl-D-galactonamide hydrogels prepared by cooling or by 3D printing.
Findings: The conditions for printing well-resolved 3D patterns have been determined for the three gelators. In imbricated structures, the solubilization of N-hexyl or N-heptyl-D-galactonamide occurred after a few hours or days and gave channels. Human mesenchymal stem cells grown on N-nonyl-D-galactonamide hydrogels prepared by heating-cooling, which are stable and have a fibrillar microstructure, developed properly. 3D printed hydrogels, which microstructure is made of micrometric flakes, appeared too fragile to withstand cell growth.

Keywords

Low molecular weight gel
Low molecular mass gel
LMWG
Molecular gel
Supramolecular
Self-assembly
Self-assembled fibers
Additive manufacturing
3D printing
Direct ink writing
Bioprinting
Cell culture
Tissue engineering

Introduction

Different kinds of biocompatible 3D printing inks are developed today. They open new perspectives to build complex 3D scaffolds for cell culture and tissue engineering [1–5]. Most of them are based on polymer, either of natural or synthetic origin. Supramolecular non-polymeric biocompatible inks, based on low molecular weight hydrogels (LMWG) are less represented. To avoid confusion between supramolecular gels based on polymers and supramolecular gels based on low molecular weight gelators, they will be called "molecular gels" in the rest of the paper. These molecules self-assemble in fibers or other kinds of anisotropic aggregates thanks to directional non-covalent interactions. Polar groups and amide

bonds of the gelators interact through hydrogen bonding. Alkyl chains and aromatic groups interact through Van der Waal interactions and π- π stacking. Both kinds of interactions between gelator molecules and between gelator molecules and solvent, drive the hydrophilic / hydrophobic segregation and lead to the self-assembly into anisotropic objects. The force of these interactions depends on the molecular structure and can give more or less dynamic assemblies. Compared with polymers, they have specificities that can be exploited to bring novelty in various applications of gels [6]. First, they are made of perfectly defined synthetic small molecules, leading to high purity and improved reproducibility of the gels. Most of the time, they have a well-defined fibrous microstructure, which is scarcely observed with polymer hydrogels. The fibers length, width, helicity etc..., vary with the structure of the gelator and can be selected on purpose. Due to the absence of covalent links in the structure, these gels are often very soft. The softness and the lack of chemical cross-links would be considered clearly as a drawback of this kind of gels, making them quite delicate. But in the context of cell culture, very soft matrices are required for some kind of cells, such as neurons. Also, the mechanical properties such as the modulus, but also the relaxation [7] or remodeling ability [8] are known to affect the cell fate. These fragile structures may be more favorable to cell migration in 3D or the formation of 3D cell assemblies (spheroids, organoids), because the cell development should be less hindered by the surrounding exogenous material [9]. In addition, in some conditions, the self-assembly can be well-controlled leading to aligned fibers and fibers tend to guide the cellular extensions [10]. Finally, the possible biochemical action and the fate of the gelator molecules in contact with cells remains largely unexplored [11],[12]. Because these small molecules are not covalently linked, the bioavailability, the interaction with cell metabolism are expected to be different compared with polymer hydrogels. Due to all these differences, molecular gels bring much novelty when they are used as a scaffold for 3D cell culture that deserves to be explored.

3D printing of molecular hydrogels is still in its infancy. Because they are very soft and non-covalent hydrogels, 3D printing methods are not easily set up and can lead to very fragile architectures. Several studies however have led to successful 3D printing of pure molecular gels, without the help of polymers (Table 1) [13],[14],[15],[16],[17]. Most of them deal with 3D printing of peptide hydrogels by "Direct Ink Writing" [18–20],[21],[22],[23],[24],[25],[13,26,27],[28]. The main application is to produce scaffolds for cell culture and demonstrate the coextrusion with cells (bioprinting). The resolution is typically in the range from a few mm down to around 200 µm [29],[30]. A lower resolution of 2 µm has been obtained by printing the dipeptide diphenylalanine with a lateral by meniscus-driven 3D printing. But in this case, the ink setting does not rely on gelation, but on solidification of the dipeptide after solvent evaporation [31]. Aside from peptides, very few other kinds of molecular gelators have been tested as inks for 3D printing, based on nucleotides/nucleosides [14],[32,33] carbohydrate [15],[34], calix[4]arenes [17] or coordination supramolecular hydrogel [35]. Table 1 recapitulates the publications describing 3D printing with low molecular weight gels, at the exclusion of polymer-LMWG mixtures. Polymer gel / molecular gel dual network mix the properties of both kinds of hydrogels [36],[37]. Because of their fragility, several studies combine peptide hydrogels and polymer hydrogels to improve notably printability [38]. But doing so, they may lose some of the advantages of molecular gels alone. A 3D printed molecular gel has also been used as a vehicle for organizing tantalum particles, improving the processing and properties of the final material [34]. Aside 3D printing, alternative methods for shaping molecular hydrogels also give valuable new techniques for controlling the self-assembly of this kind of hydrogels [39],[40],[41,42].

In 3D printing relying on simple extrusion or "Direct Ink Writing", without photocrosslinking, keeping a good shape fidelity and resolution relies on different mechanisms [29,30,43–46]. First, working with highly viscous inks helps avoid a large spreading of the ink before complete gelation. Then, complete gelation of the ink occurs either by cooling and/or by chemical or biochemical reaction and/or by solvent exchange (coagulation) and/or by gel network reorganization (thixotropy). These triggers operate with different timescales. Cooling and solvent exchange can be very fast while thixotropy and chemical reactions are most of the time slower phenomena. Thixotropy is highly desirable since it has the advantage of being the most compatible with cell survival, therefore, with bioprinting. The resolution and shape fidelity will result from the combination of ink spreading -linked to viscosity- and ink setting rate. They tend to be antagonistic, e.g. a high viscosity will impair the diffusion of reagents or solvents and will slower down thixotropic recover. An appropriate compromise must be found.

Carbohydrate-derived hydrogels are under-represented in this application, because carbohydrate derivatives are more difficult to synthetize compared with peptides. However, carbohydrate molecular gels easy to synthesize do exist and could be an interesting alternative to peptide hydrogels, notably as scaffolds for cell culture [9,14,16,47–52]. They also have a well-defined molecular structure, high purity and will bring many differences in contact with cells. The differences can come from the microstructure, the mechanical properties, the network porosity, the chemical composition, the degradation products. Mixing both peptides and carbohydrate molecular gels would be even more relevant for mimicking the chemical composition of the extracellular matrix. We work with carbohydrate molecular gels based on aldonic, sugar acids linked to aliphatic amines (Fig. 1). Changing the aldonic acid configuration, the chain length of the fatty chain and the nature of the linker (e.g. amide, urea or glycine) gives rise to hydrogels with various properties and microstructures [40,48,49]. Different gelation methods can also be implemented [9,15,40,41]. By solvent exchange, the gelation is triggered by injecting a solution of the gelator in dimethylsulfoxide (DMSO) in water [15,40,41]. The low solubility of the gelator in water leads to very fast self-assembly in contact with water. We have shown that an ink composed of N-heptyl-D-galactonamide (25 to 40 mg/mL) can be 3D printed by direct ink writing in well-defined patterns [15]. The objective of the present study is to extend the method to other carbohydrate molecular gels and to determine the parameters affecting the resolution (printing speed, extrusion rate of the ink, concentration, solubility of the gelator). In addition to N-heptyl-D-galactonamide, three new gelators of the same family have been studied: N-hexyl-D-galactonamide, N-octyl-D-galactonamide and N-nonyl-D-galactonamide (Fig. 1). We were also considering the possibility to fabricate 3D printed structures more or less persistent by playing on the solubility of the gelator. The structures printed with N-heptyl-D-galactonamide tend to dissolve within a few days post-printing. It can therefore be used as sacrificial ink. We expected that by increasing the length of the alkyl chain, the solubility of the gel in water decreases, leading to structures that will persist in water for a long time. By alternating soluble and not soluble 3D printed structures, it should be possible to create imbricated architectures and channels. For that, two conditions must be fulfilled: the persistent ink must not diffuse into the sacrificial ink layers, and it must be free-standing after the sacrificial ink removal. These hypotheses have been tested in this study.

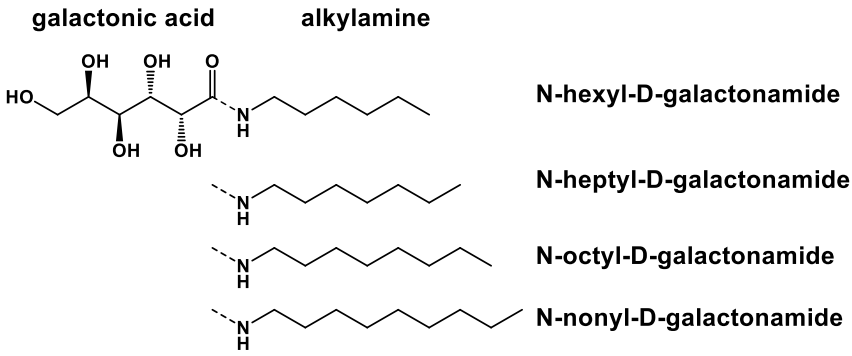

Fig. 1. Molecular structure of the gelators

Table 1. Review table on 3D printing of Low Molecular Weight Gels, up to 2021

LMWG composition	3D printing and gelation technique	Bioprinting (coextrusion with cells)	Cell culture	Type of architecture, resolution** Comments	[reference] Year
EARLY ATTEMPTS (gel extrusion without true 3D printing)					
Lysine tri- to hexa-peptides	Extrusion in saline bath	no*	yes	hydrogel noodles and droplets not spatially organized	[53] 2015
Calix(4)arene molecular organogels in organosilanes and carbon tetrachloride	Extrusion at air of a viscous thixotropic hydrogel paste			hydrogel noodles; line width ≈3 mm	[17] 2016
PEPTIDES					
Diphenylalanine gelators, including Fmoc-diphenylalanine (FmocFF)	Extrusion at air, gelation by DMSO/water mixing or pH change	no	no	hydrogel frames and lines line width ≈3,5 mm	[19] 2017 [24] 2021
PeptiGel (Manchester Biogel) Alpha1 and AlphaProB	Extrusion at air, viscosity control	yes	yes	hydrogel mesh line width ≈250 µm	[18] 2017
Fmoc-Tyrosine-aspartic acid (Fmoc-YD) + Fmoc-Tyrosine-Lysine (Fmoc-YK)	Droplet printing, fast gelation by opposite charge interaction	no*	yes	hydrogel mesh line width ≈ 250 µm	[21] 2019
FmocFF + gold and silver nanoparticles	Extrusion, gelation by DMSO-water mixing	no	no	lines, line width ≈ 1.9 mm For detection applications	[13] 2019
Tetrapeptides (IIFK / IIZK)	Co-axial extrusion with PBS and viscosity control	yes	yes	3D printed cylinders > 1 cm height, nose model. Wall thickness: ≈ 1 mm	[22] 2021
Tetrapeptides (IVZK / IVFK)	Co-axial extrusion with PBS and viscosity control	yes	yes	hydrogel mesh; line width ≈ 800 µm	[23] 2021
Biogel X peptide hydrogel	Extrusion at air and room temperature	-	yes	providers' websites	
Nonapeptide amphiphiles and chromophore amphiphile	Extrusion at air, gelation by ionic cross-linking on salt-coated substrates	yes	yes	lines; line width ≈ 300 and 100 µm + peptide fibers aligned during extrusion	[25] 2021
Assembling peptide but not gel: Diphenylalanine	Meniscus-guided 3D printing at air solidification by fast solvent evaporation at 70°C	no	no	Not a gel but solid FF. Complex shapes, high resolution: 2 µm. Piezoelectric	[31] 2021

CARBOHYDRATES, NUCLEOSIDES/-TIDES					
Guanosine (G) - arylboronate - K^+	Extrusion at air, viscosity control and thixotropy, gelation by G-K^+ quadruplex and boronate esters	yes	yes	Hydrogel lines and mesh	[33] 2018
Cytidine (C)- borate - Ag^+	Extrusion at air, viscosity control and thixotropy, gelation by C-Ag^+ complex and borate esters	no	no but wound healing	Hydrogel "E" letter	[32] 2019
Dibenzylidene sorbitol in butanol + tantalum particles	Extrusion at air, gelation by cooling hot LMWG + Tantalum powder slurry	no	no	LMWG acts as a structural support for printing tantalum; line width = 630 µm	[34] 2019
N-heptyl-D-galactonamide	Extrusion in water, gelation by DMSO-water solvent exchange	no	no	hydrogel frames and lines, line width ≈ 600 µm	[15] 2020
Thymidine grafted phospholipid	Extrusion at air, viscosity control, gelation by thixotropy recovery	yes	yes	hydrogel mesh; line width ≈ 3 mm	[14] 2020
Glucosamine benzylidene derivatives	Extrusion at air, viscosity control with composition	no	no	Line with controlled extrusion rate of the gel (no spatial control in 3D); line width ≈ 3 mm	[52] 2021
Benzylidene sorbitol acylhydrazide derivative	Extrusion in water, gelation by DMSO-water solvent exchange	no	yes	hydrogel “E” letter with various spacing, line width ≈ 700 µm (10 layers)	[16] 2022
N-alkyl-D-galactonamides	Extrusion in water, gelation by DMSO-water solvent exchange	no	no	hydrogel “F” letter with various spacing, up to 10 layers, best line width ≈ 330 µm (1 layer); 700 µm (10 layers)	This work
OTHERS					
Folate-Zn^{2+}	Extrusion at air or in solution, viscosity control and thixotropy, Gelation by coordination reaction	yes	yes	Hydrogel patterns; Line width ≈ 4 mm	[35] 2018
Bis-imidazolium amphiphile + acrylate monomers	Extrusion at air, gelation by fast thixotropy recovery of the supramolecular gel. LMWG = structural support for printing free monomers	no	no	hydrogel lines, line width ≈ 350 µm photocrosslinking after 3D printing, double network	[36] 2021

* seeded after printing

** approximate values have been determined from images provided in the publications. Most of the time they have not been explicitly given by the authors. So, the measure has been worked out from the thinner structures found in the Figures.

Materials and methods

N-hexyl, N-octyl and N-nonyl-D-galactonamides have been synthetized as previously described in: Chalard et al. 2018 [9]. Molecular weights are respectively: 279.33 (GalC6); 293.36 (GalC7); 307.39 (GalC8); 321.41 (GalC9). N-heptyl-D-galactonamide has been purchased from Innov'Orga. Non-anhydrous dimethylsulfoxide > 99% from Fisher has been used for printing assays.

Gelator solutions

Solutions of gelators have been prepared by dissolving the gelator in non-anhydrous DMSO at the concentration described in the main text. A 1% solution means dissolving 10 mg of the gelator in 1 mL of DMSO. All gelators readily dissolved in DMSO at room temperature. For GalC8 and GalC9, a longer time (around 10 min) can be needed for complete dissolution. Ultrasonication can be used also to help dissolution. The vials are selected so that the tip of the printed needle can reach the bottom of the vial to take off the whole solution if needed. For fluorescent prints, fluorospheres have been added to the gel solution. Green fluorospheres are polystyrene microspheres of diameter 1 µm yellow-green (ex/em: 505/510). Red fluorospheres are polystyrene microspheres of diameter 1 µm yellow-green (ex/em: 580/605). The microspheres suspension is diluted at 1/10 and 100 µL is added in 1 mL of the gelator solution in DMSO.

3D printed patterns with Axidraw (1-layer and 10-layers "F")

For 3D-printing, a drawing/writing robot, Axidraw V3, was coupled to a syringe pump from Chemyx Inc. (Model Fusion 100CR) (Fig. 1). The drawing machine moved along the XY axes, controlled by the software Inkscape. The Z-axis height was changed manually by using a Z moving platform. The pattern was drawn in Inkscape. The number of layers is determined by stacking as many replicates of the initial pattern as desired on the Inkscape drawing. Replicates (and not copy/paste) are drawn in continuity to each other without pen lift between replicates. The Axidraw control plugin in Inksape makes it possible to control the velocity of the drawing machine, the nozzle moves up and down and which pattern is printed. The relation between % velocity and true velocity is given in the specifications provided by the manufacturer. It has been checked with a chronometer while drawing a 24 cm straight line. 1% - 2% - 3% velocity stands for 2 mm/s - 4 mm/s - 6 mm/s respectively. The drawing is made at a constant speed (setting: "use constant speed when pen is down"). Before printing, the tip height is set at 300 µm, by stacking three cover slides (each having a thickness of 100 µm) and by setting the "pen height" in the Axidraw plugin to have contact between the tip and the cover slide. The cover slides are then removed, letting a space of 300 µm. Before printing, blank drawings are tested to place the patterns conveniently in space. A set square and spirit level are used to refine the relative position of the Axidraw the Z-moving platform and the drawing space.

For "F patterns" designed for testing the inks and drawing conditions, the drawing is made in 8 cm diameter polystyrene Petri dishes, filled with 25 mL of ultrapure water at room temperature. The gelator solutions were extruded in the water bath, setting the distance between the tip and the drawing surface at 300 µm. The syringe is filled with the gelator solution and adapted to the syringe pump and the Axidraw pen holder with tubing and luer-lock needle adapters. The absence of bubbles in the tubing and needle is checked. One drop of solution is brought just at the exit of the nozzle, then wiped out. Any solution hanging out of the nozzle may compromise the quality of printing and must be removed before printing. Blunt-tip needles 30G (ID 160 µm) gauges have been used.

Width and spacing of gel deposit were measured using DinoLite digital microscope (model AM7515MZTL, white light or model AM4115T-GRFBY green/red fluorescence) with its corresponding software. For the study of the influence of printing speed and extrusion flow rate on the width of gel deposit, measurements have been taken at the same positions for every printing.

Cell culture assays

3D printed and thermal gels in 8-well culture chamber slides

3D printing in 8-well culture chamber slides (Labteck) has been performed in a PSM hood. Tubing and needles are sterilized with alcohol and allowed to dry before printing. To ensure better stability of the printed structures and to get a continuous gel surface, a pattern made of tight lines spaced 500 µm apart from each other has been drawn in the wells of an 8-well culture chamber slide in 30 layers. The pattern is 7 mm x 6 mm wide. A N-nonyl-D-galactonamide solution (GalC9, MW = 321.37) containing 10 mg in 1 mL of dimethylsulfoxide (DMSO) in extruded at 7.5 µL/min and printed at 4 mm/s. The z platform is moved down 75 µm/layer. Printing is made in a well filled with 1 mL of sterile water. The total amount of GalC9 in the 3D printing wells is 2.25 mg (0.007 mmol). The total volume of DMSO is 225 µL of DMSO. Besides, gels obtained by cooling are prepared by dissolving 10 mg of GalC9 in 1 mL of water at 130°C in a sealed vial. After cooling, the gel is removed with a spatula and poured into a labteck well. The total amount of GalC9 in these wells is 10 mg (0.031 mmol). To replace water with a physiological medium and remove DMSO, all the gels are rinsed by taking off the supernatant and adding PBS. Rinsing is first made twice by removing only half of the volume of liquid and adding half of the volume with PBS, then twice by removing the maximum of liquid and replacing it with 1 mL of PBS. The duration of rinsing is at least 15 min each time. In 3D printed gels, fragments dissociate at the periphery during rinsing, but the centers stay cohesive. Conversely, gels prepared by cooling are very cohesive, they do not dissociate at all upon rinsing. Because the volume of the gels prepared by cooling is larger compared with 3D printed gels, they have been rinsed twice more times with 1 mL of PBS (4 times). After rinsing, PBS is taken off and replaced by culture medium (α-MEM with 10% FBS) and left overnight before seeding the cells.

Isolation of hMSC, cell culture and cell viability assay

Human mesenchymal stem cells (hMSC) derived from white adipose tissue were obtained from abdominal dermolipectomy of donors undergoing cosmetic surgery as previously described [54]. In brief, the stroma vascular fraction containing MSC were isolated by NB4 collagenase digestion, cells were resuspended in α-MEM (Life-Technologies, UK), supplemented with 0.1% (v/v) amphotericin B, 1% (v/v) streptomycin/penicillin and 10% FBS, and seeded at 4000 cells/cm² for amplification. After 7 days, MSC were trypsinized and seeded 30 000 cells/well on GalC9 hydrogel 3D printed, or prepared by cooling, in the 8 well chamber slide. After 7 days of culture in α-MEM 10% FBS, fluorescent live–dead staining assay (Molecular probe) was used according to the manufacturer instructions to visualize the proportion of viable cells in green (calcein AM) and nonviable cells in red (ethidium homodimer-1). Samples were analyzed by confocal microscopy (LSM 880, Carl Zeiss, France) and images were processed using Fiji software (National Institutes of Health, USA).

3D printing of imbricated structures

3D printing of imbricated structures has been performed with the same experimental set as the previous 3D printing of “F” patterns. The pattern of the imbricated structures, shown in Fig.7a, has been drawn in Inkscape. A continuous pattern is required, since the syringe flow pump and the

Axidraw are not coupled. The ink is continuously extruded regardless of the Axidraw movement. Therefore, the pattern designed to print imbricated structures is composed of three full squares connected to each other by connecting lines. Ten layers of this pattern were printed with a persistent ink to form the foundation of the structure. The connecting lines were then cut manually to enable the insertion of an empty square around the central full square. Using sacrificial ink, at least ten layers of the empty square pattern were printed until reaching the height of the structure foundation (the number of layers has been adapted depending on the gelator, see Table 4). Then ten layers of a full rectangle recovering the whole structure were printed with the same persistent ink used for printing the structure foundation. The printing of these structures was performed inside 8 cm diameter polystyrene Petri dishes, filled with 25 mL of ultrapure water at room temperature. Blunt-tip needles of 30G (ID 160 µm) gauges have been used.

Electron microscopy

Cryo-scanning electron microscopy (Cryo-SEM) of GalC6, GalC8 and GalC9 3D printed hydrogels have been made after high-pressure freezing (HPF) as follow: a piece of the 3D printed hydrogel is cut and is inserted between two HPF specimen carriers dedicated for cryofracture (Leica) and it is loaded immediately into an ICE HPF machine (Leica). The sample is fixated and frozen within 5 ms at 2050 bar and samples are then transferred to cryovials under liquid nitrogen. Then HPF specimen carrier with freeze solution is inserted for the preparation chamber Quorum PP3000T. For insertion, specimen shuttle cryo stubs and HPF specimen carrier adapter suitable is used follow the description of B. Payre and coll. in ref [55]. After the quick transfer under vacuum in the preparation chamber, the samples were fractured at -140°C, sublimed at -95°C for 60 min and then coated by platinum sputtering. They were at last transferred in the cryo-SEM Quanta 250 FEG chamber and kept at -140°C for observation with a FEI Quanta 250 FEG scanning electron microscope at an accelerating voltage of 5kV. Cryogenization of GalC7 3D printed hydrogel has been made differently: a piece of the printed gel is deposited on the cryo-SEM cane and frozen at −220 °C in liquid nitrogen. The frozen sample was put at −145 °C under vacuum in the cryo-transfer system chamber (Quorum PP3000 T) without fracturing. The freeze-drying was performed at −95 °C for 60 min, then the sample is coated by platinum sputtering and introduced in the microscope chamber. Observations are made in the same conditions as described above for GalC6, GalC8 and GalC9.

Solubility

GalC6, GalC7, GalC8 and GalC9 powder have been weighted in an NMR tube (amounts from 0.6 to 3 mg for GalC6 to reach below and above saturation; 1 to 2 mg for the other gelators, corresponding to saturation in all cases). 500 µL of a solution of D_2O (11.045 g) + DMSO (0.053 g) is added (the same solution for all the tubes). Thus, 500 µL of this solution contains 552 mg of D_2O and 2.65 mg of DMSO. Tubes have been either heated for 10 min at 100°C, or stayed at room temperature (20°C) until measurement in NMR spectrometer at 25°C. Then the NMR spectra have been recorded after 48h (2 days), 110h (5 days), 238h (10 days) to check if the solubilized amount measured corresponds to equilibrium. All measurements gave similar values, showing that whatever the method of preparation, the amount measured after 48h is stable. It gives the solubility value. Except for GalC6 samples below 5 mg/mL, all samples still contain fragments of gelator not solubilized, and are thus at saturation. The sensitivity of the spectrometer did not enable to reach routinely the values under saturation for the other gelators. NMR spectra have been performed on a 300 MHz spectrometer (Brüker) with the following parameters: 128 scans for GalC6 to GalC8 and 256 scans for GalC9, D1 = 5s. The spectrum phase correction and the slope and bias correction of integrals have been made with accuracy, since it is critical for the accuracy of the measurement. The difference of concentration

measured by weighting and by NMS for samples under saturation obtained with GalC6 is between 7 to 25%.

Results and discussion

1- 3D printing conditions for N-hexyl, N-octyl and N-nonyl-D-galactonamides

3D printing of alkyl-galactonamide hydrogels is performed by injecting a solution of the gelators in dimethylsulfoxide (DMSO) at room temperature in a bath of water. Since these inks are non-viscous liquids, the bath must not move to avoid the deformation of the ink jet. As a result, 3D printers devoted to the 3D printing of fused materials available in the mainstream market are not convenient for this application. Conversely, bioprinters, which can take in charge of printing in more various conditions, are compatible but they are quite expensive. For these reasons, in this study, 3D printing has been performed with a drawing robot whose writing speed can be set in the adapted range (Axidraw). It has been coupled to a syringe pump and a Z-moving manual platform (Fig. 2a). Stepwise manual movements in Z are not disturbing, because they are very slow. This set represents cheap but adequate equipment for the chemists for testing new 3D printing inks.

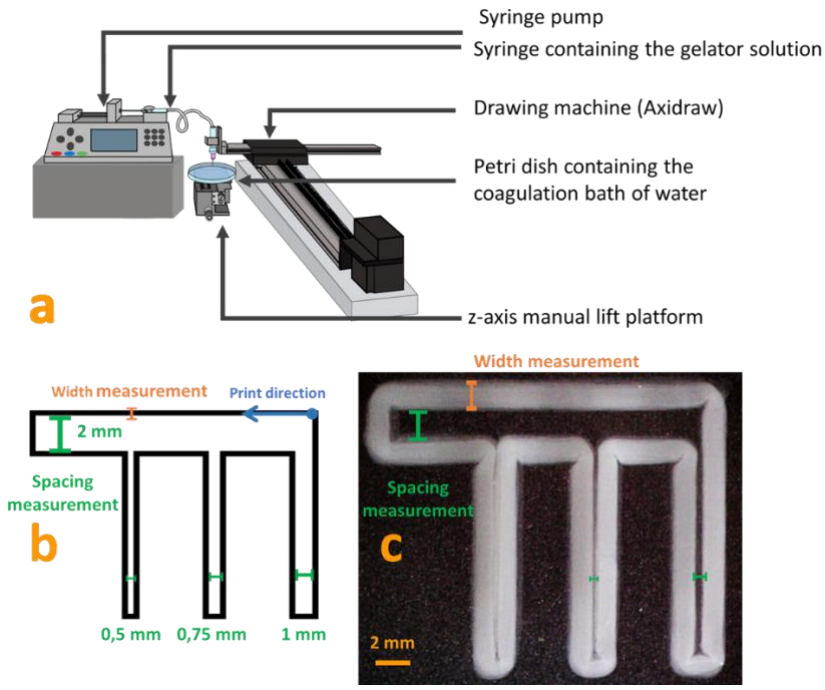

Fig. 2. (a) 3D printing equipment and (b) pattern design with (c) a picture of an actual print.

For printing N-hexyl (GalC6), N-heptyl (GalC7), N-octyl (GalC8) and N-nonyl (GalC9) D-galactonamides, a solution of the gelator in dimethylsulfoxide (concentrations from 1 to 5 wt%) is injected in a bath of water in a polystyrene Petri dish filled with 25 mL of water. The extrusion rate is set at 5 – 7.5 – 10 - 15 µL/min and the printing speed at 2 - 4 - 6 mm/s. The needle is placed very close to the surface (300 µm) to ensure good adhesion of the gel on the polystyrene surface. When the distance is higher, the gel has already partly set when it comes in contact with the polystyrene dish, which impairs adhesion. The extrusion rate is selected in a range adapted to the writing speed and in the range in which clogging is avoided. Actually, at low extrusion rates the gel tends to clog at the exit of the needle. The less soluble is the gelator, the longer is the alkyl chain, the more the gel tends to

clog. Clogging can be most often avoided by increasing the printing speed, the extrusion rate and the nozzle-printed layer distance. Preliminary experiments enabled to select the concentrations of gelator in DMSO adapted to 3D printing, which are 5 wt% (50 mg/mL) for GalC6, 2.5 wt% (25 mg/mL) for GalC7 [15] and 1 wt% (10 mg/mL) for GalC8 and GalC9. These concentrations are high enough to give a consistent gel that sets quickly and not too high to avoid the gel clogging at the nozzle. The concentration of GalC6 needs to be increased at 5 wt% because with inks at 2.5 wt%, the pattern dissolved in the water bath very quickly. Conversely, GalC8 and GalC9 are less soluble in water compared with GalC6 and GalC7, so they set very quickly in contact with water. Using lower concentrations, typically 1 wt%, avoids clogging.

To study the quality of the printed patterns, one-layer patterns and ten-layers patterns have been drawn with each gel. To test the shape fidelity and the resolution obtained with the different inks in different conditions, a pattern in which the spacings between the lines are 2 mm, 1 mm, 750 µm and 500 µm and with straight angles has been drawn (Fig. 2b). On the one-layered patterns, the **width** of the gel lines and the **spacing** (empty space between two gel lines) have been measured under all the conditions tested. The complete data are reported in Supporting Material SI-1(Fig. SI-1.1 to SI-1.4). In Table 2 have been gathered the best conditions for each gelator, namely, the conditions giving the best resolution, the thinnest lines and the most regular patterns. Examples of patterns with the thinnest width and/or the best resolution and the worst resolution for each gelator are shown in Fig. 3a,b respectively and in Fig. SI-2.1 to SI-2.3. The best conditions are found mostly by adjusting the extrusion rate. A too fast extrusion rate leads to the delivery of an excess of ink, leading to the enlargement of the pattern. Conversely, a too low extrusion rate can lead to gel clogging. At medium conditions, typically with a printing speed of 4 mm/s and an extrusion rate of 5 µl/min or 7.5 µL/ min, the three gelator GalC7, GalC8 and GalC9 can be printed and give well-resolved patterns. With GalC6, because the solution in DMSO is more concentrated (5 wt%), the extrusion rate needs to be increased to 10 µL/min to avoid clogging.

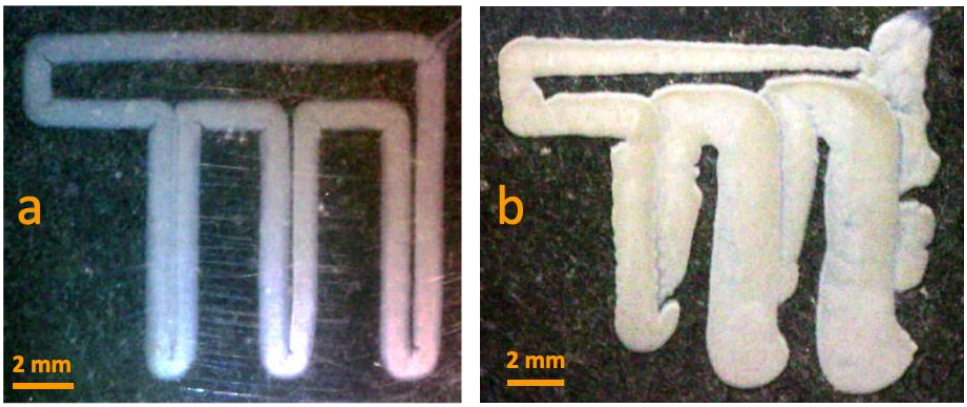

Fig. 3. Example of patterns with good resolution and bad resolution obtained with (a) GalC9 1wt% 6mm/s 7.5 µL/min; (b) GalC9 1wt% 2mm/s 15 µL/min. Similar comparison is given in SI-2 for GalC6, GalC7 and GalC8.

To quantify the quality of the patterns, for each condition the width of the gel deposit was measured at the same points. 22 points of measurement, designated as “Positions" have been selected along the pattern and are shown in Fig. SI-3.1. These positions are numbered following the printing path. A mean of the 22 widths measured and the smallest width out of these 22 positions are reported in Table 2. Typical pattern widths with these inks are in the range of 600 to 900 µm for 1 layer and 1 mm to 1.5 mm for 10 layers. The best resolution observed was 330 µm with one layer of GalC9 1 wt% at 7.5

µL/min and 2 mm/s. This resolution was however not constant all over the pattern (see Fig. SI-3.2). To know if the width irregularity along a pattern was systematic or not, we gathered all the measurements of the widths of one-layered gel deposit in a heatmap analyzing the width on 22 positions (Fig. 4). The green color represents the thinner gel lines while the red color represents the larger gel lines. Generally, larger gel deposits (in red) are observed at a printing speed of 2 mm/s and an extrusion rate of 20 µL/min for all gelators. Thinner gel deposits are mainly observed at a printing speed of 4 mm/s and/or 6 mm/s and an extrusion rate of 5 µL/min, except for GalC6, where clogging issues were encountered at these conditions. This tendency is expected, since the pattern is enlarged when the volume of ink delivered per surface unit increases [15]. This tendency is also illustrated in the graphs giving the relation between the extrusion rate and the pattern width at one position (Fig. SI-3.3 to SI-3.5). The heating map also shows that GalC9 tends to give systematically thinner patterns, which is related to the very fast setting of this gelator, due to its very low solubility in water (see section 4). More in detail, the heating map also revealed that repeatedly, in some positions (positions 8, 9, 14,15, 20, 21), the gel deposit tends to be thinner compared with the rest of the pattern. These positions correspond to the lines coming back parallel to a line that has just been written, at less than 1 mm of distance. It may be mainly due to the fact that the ink is stopped by the line of the gel already set, making this second line thinner. A last method of multivariate analysis was applied to the width measurements: on each of the 22 positions, the number of times that the minimum or the maximum width has been recorded for this position has been counted. The results are reported in Table SI-3.6. It shows that the gel deposit tends to be thinner at the beginning of the print and enlarges wider and wider until the end of the print. This phenomenon can be due to the fact the proportion of DMSO around the pattern increases all along the print. DMSO may decrease the speed of self-assembly of the gelators by increasing the solubility locally in a DMSO/water mixture. This assumption is also supported by the fact that this phenomenon is mostly observed when the extrusion rate is high, dispensing much larger volumes of DMSO. This tendency can also be seen on the heatmap (Fig. 4).

Table 2. Best 3D printing conditions for N-alkyl-D-galactonamide hydrogels and resulting line widths

	Gelator	Printing speed (mm/s)	Extrusion rate (µL /min)	Mean width of well-defined patterns (mm)	Smallest width observed (mm)
1 layer	GalC6 5 wt%	4	10	0.617	0.449
		6	20	0.872	0.691
	GalC7 2.5 wt%	4	5	0.771	0.558
		6	5	0.788	0.490
	GalC8 1 wt%	6	5	0.822	0.653
	GalC9 1 wt%	2	7,5	0.667	0.332*
		6	7,5	0.903	0.817
10 layers	GalC6 5 wt%	4	10	1.565	1.338
	GalC7 2.5 wt%	4	5	1.203	1.013
	GalC8 1 wt%	6	5	1.310	1.121
	GalC9 1 wt%	6	5	1.062	0.702

In this Table are analyzed the more regular patterns observed with the different hydrogels and printing conditions, either in 1 layer or 10 layers. "Mean width" is calculated as the mean of widths measured on 22 positions along the pattern (see SI-3.1 for the location of the 22 positions). "Smaller width" represents the smaller value out of these 22 positions.
** represents the smallest width that has been reached. However, this condition has not been considered as the best printing condition due to irregular widths in other parts of the pattern (see Fig. SI-3.2)*

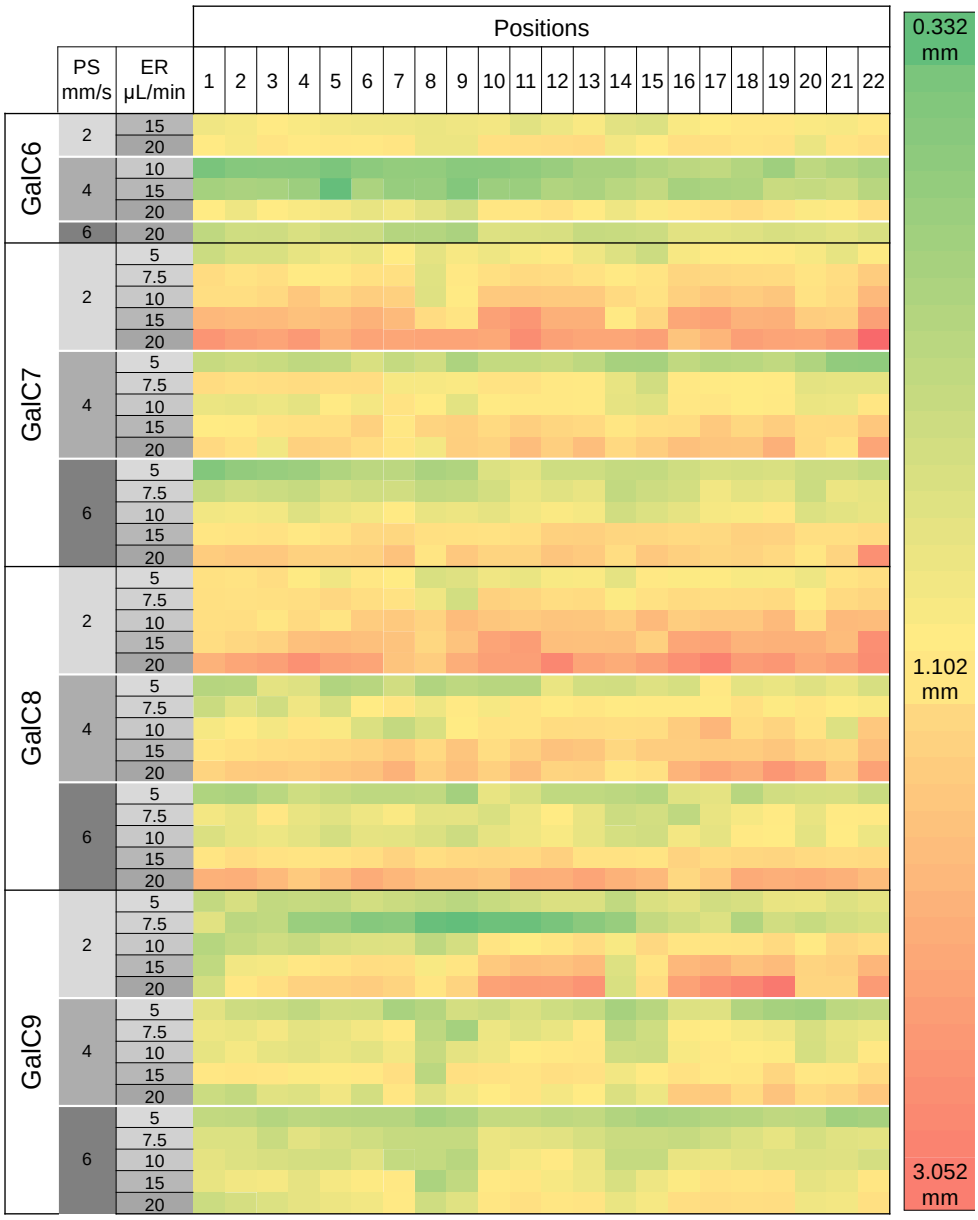

Fig. 4. Heatmap of widths of one-layered gel deposit. Cells are colored according to the measured width, in green for low values and red for high values. The measurements are grouped on the y-axis by gelator and by conditions (PS: printing speed (mm/s), ER: extrusion rate (µL/min). The heatmap chart was generated by using conditional formatting in MS Excel.

2- Ten layers prints

The shape fidelity has also been tested for the four gels on a 10 layers pattern, in the best conditions selected from the preceding study (Fig. 5). As far as GalC9 is concerned, a small adaptation of the extrusion rate was needed, which was decreased from 7.5 µl/min to 5 µL/min. Indeed, the behavior of the gel slightly changes when printing multiple layers compared to the printing of a single layer. It may be due to the vicinity of the first layer which impacts the printing conditions of the second and subsequent layers. During the printing of the 10 layers, the Z-moving platform is moved down stepwise manually, around 75 µm/layer. This value corresponds to the height measured for a one-layer deposit of GalC7 [15].

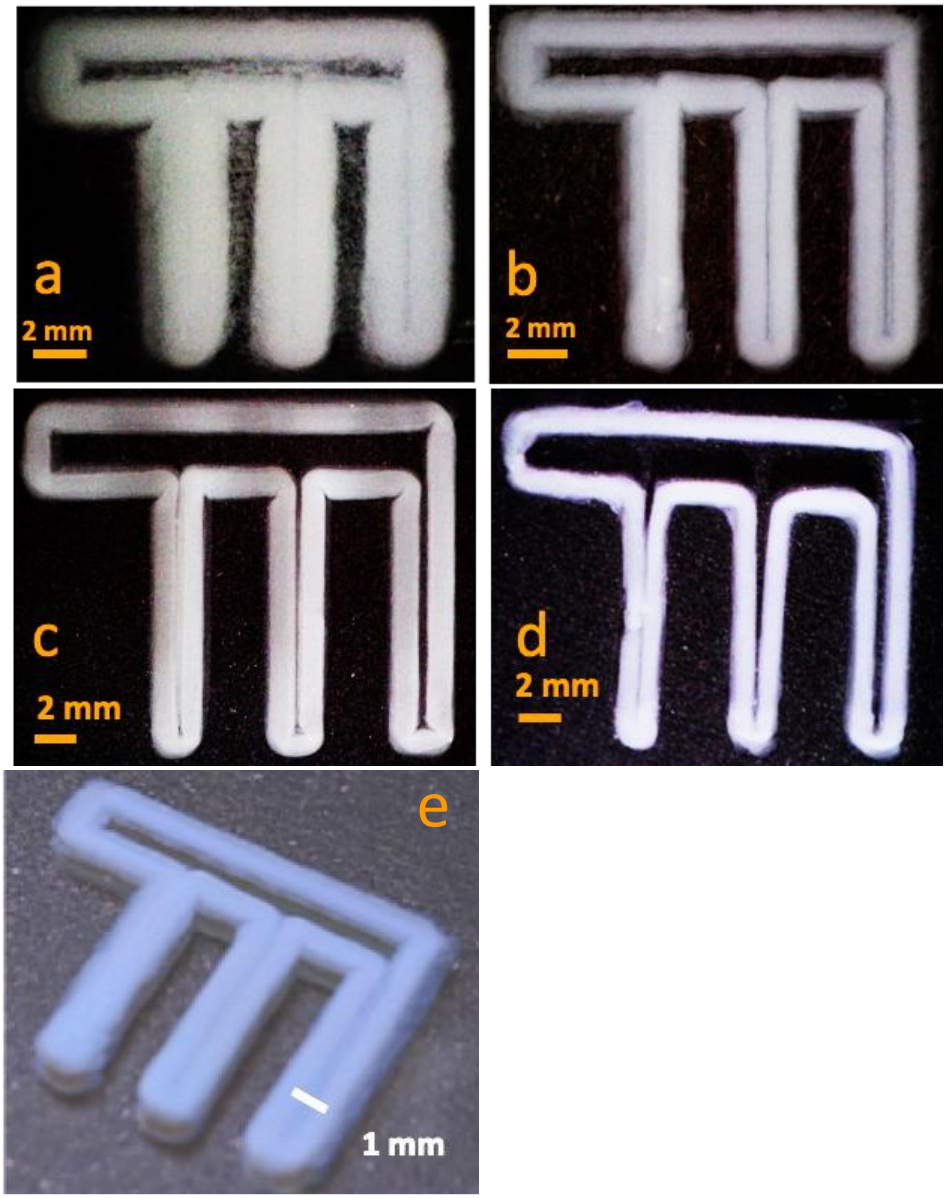

Fig. 5. Ten layers print (a): GalC6 5wt% (4mm/s, 10 µL/min); (b): GalC7 2.5wt% (4mm/s, 5µL/min); (c): GalC8: 1wt% (6mm/s, 5µL/min); (d) GalC9: 1wt% (6mm/s, 5 µL/min); (e) 3D view of a 10 layers print with GalC7 2.5wt%.

The width of the pattern decreases with the solubility of the gelator, which decreases when the length of the fatty chain increases, in the order GalC6 (1.6 mm) > GalC7 ≈ GalC8 (1.3 mm) > GalC9 (1.1 mm) (mean width over the 22 positions). The smaller width for 10 layers (700 µm) is obtained with GalC9 (Table 2). This trend is related to the fact that the less soluble is the gelator, the faster it sets in contact with water, thus giving a thinner pattern. However, the fast setting of GalC9 can be a drawback while stacking layers since the layers are less likely to adhere to one another.

3- Microstructure

The microstructure of the 3D printed gels has been observed by Cryo Scanning Electron Microscopy (cryo-SEM). We observed that the two galactonamides with the shorter alkyl chains GalC6 and GalC7 give 3D printed hydrogels with a fibrous microstructure. The self-assembled fibers are more than tenth microns length. The two galactonamides with the longer alkyl chains GalC8 and GalC9 give 3D printed hydrogels formed of very short flat ribbons, shorter than 5 microns length. They merely look

like flakes with more or less the same dimension in width and length (Fig. 6). These differences in microstructure are likely to have an impact on the gel cohesion. The supramolecular fiber formation and other mechanisms related, such as branching, are linked to the supersaturation of the gelator in solution. By increasing the chain length, the solubility of the gelator decreases, affecting the availability of free gelator molecules in solution, impairing the fiber growth on long distances [56],[57].

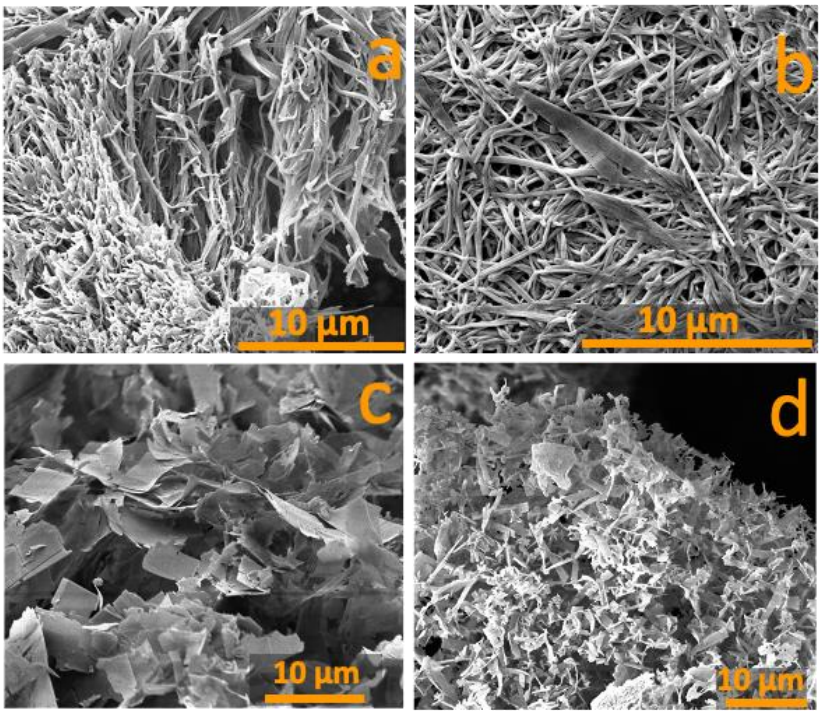

Gel	GalC6	GalC7	GalC8	GalC9
Average fiber width (µm)	0.28	0.17	3.39	0.69

Fig. 6. CryoSEM giving the microstructure of the 3D printed hydrogels: (a) GalC6; (b) GalC7; (c) GalC8; (d) GalC9 scale bar = 10 µm and mean fibers width table.

4- Solubility

After printing the 10-layers patterns, we observed that the GalC6 and GalC7 patterns tend to dissolve in few hours or days in the bath of water in which they have been printed. This observation about dissolution rose the question of quantifying the solubilities of the four alkyl-D-galactonamides. For this purpose, the concentration of free gelator in equilibrium with the gel or solid-state has been measured by NMR. The measured solubility corresponds to the solubility of the gelators in D_2O. In surfactant systems, D_2O is known to make stronger hydrogen bonds which tends to lower the Critical Micellar Concentration (CMC) compared with CMC in H_2O. Thus, the quantity of free molecules is expected to be lower in D_2O compared with H_2O. This trend increases with the alkyl chain length [58]. It must be taken into consideration in the results. However, we preferred this method which gives a direct measurement of the free molecules without manipulating the samples. Measuring the solubility in H_2O involves taking off the aqueous phase, filtrating this solution to remove the small self-assembled aggregates and water removal. All these steps tend to increase the inaccuracy. Also, we cannot be sure that only free molecules are measured, since small aggregates can pass through the filter. The N-alkyl-D-galactonamides / water mixtures have been prepared directly in NMR tubes at

different concentrations in D_2O and DMSO was added as an internal standard. After 2 days, 5 days and 10 days at 20°C (after preparation by a 10 min heating or only at room temperature), the presence of a gel or any solid structure is assessed by visual inspection and NMR spectrum is recorded. Well-resolved signals have been obtained for all the gelators whatever the concentration and the presence of gel. These signals have been assigned to the free gelator fraction and quantified. The fraction of gelator molecules self-assembled in fibers or in solid form does not give any observable signal [59]. In saturated samples, for every gelator, all the concentrations measured by NMR were close to each other, whatever the method of preparation and equilibration time. The mean value, corresponding to the solubility is given in Table 3. By decreasing the concentration, for the most soluble gelator GalC6, it was possible to measure the concentration of dilute solutions, below the gelation threshold. On those samples, the difference between concentrations calculated from weighing and the concentrations measured by NMR varied from 7 to 25%. For less soluble gelators, it was not possible to get the measure at a low concentration. The quantities involved are below the balance and/or NMR resolution and the mixtures are heterogeneous (solid gelator + water). It precluded the preparation of low concentration samples by dilution.

Table 3. Solubility of N-hexyl, N-heptyl, N-octyl, N-nonyl-D-galactonamides

Gel		GalC6	GalC7	GalC8	GalC9
Solubility (µmol/mL)	NMR (in D_2O)	5.3	1.2	0.3	0.07
	TGA (in H_2O)	5.0	1.2	0.7	-

The solubilities measured by NMR have been also compared with previous results obtained for GalC6, GalC7 and GalC8 by thermogravimetric analysis (TGA) [9] (Table 3). With this technique, a gel was prepared in H_2O by the same method as described for NMR. After 21h, the gel was compressed and the aqueous phase was filtrated at 220 nm. The ratio between the water and the solid fraction of the filtrate was then measured by TGA. A quite good correlation between the two kinds of measurements was obtained. It confirmed the solubility values and the relevance of the methods used, despite the specificities of each method discussed above.

These measurements also revealed that quite unexpectedly, the hydrolysis of the amide bond occurs quite easily upon heating. Even though neither base nor acid are added, after 20 minutes of heating at 100°C, new signals start to be observed in NMR and increased with the heating time. They correspond to the alkylammonium. This assignment is confirmed by a peak corresponding to the alkylammonium in mass spectrometry. Also, a new doublet for the C2 of the carbohydrate (-CHOH-CONH) is also seen -0.17 ppm upfield, while the other carbohydrate signals are not strongly affected, in accordance with the hypothesis of a simple hydrolysis (see SI-4).

5- Imbricated structures and channels using soluble and persistent N-alkyl-D-galactonamides

Taking advantage of the quite fast dissolution of GalC6 and GalC7 patterns, we used these two hydrogels as sacrificial inks to test the possibility to form channels. When the gel is deposited during printing, it is not at the thermodynamic equilibrium. Then the pattern slowly dissolves to reach the solubility equilibrium in the 25 mL of pure water, leading in some cases to complete dissolution.

To perform the experiments, we printed imbricated structures using either GalC6 or GalC7 as the sacrificial inks and GalC9 as a persistent ink. A first pattern of three full squares has been printed with 10 layers of GalC9. Then an empty square has been printed with either GalC6 or GalC7 around the GalC9 middle square (10 layers of 2.5% GalC7 or 60 layers of 1% GalC7 or 20 layers of 5% GalC6 are needed to reach the level of the GalC9 hydrogel). Then a third pattern, a full rectangle, is printed

with GalC9 on the top of the whole structure, in 10 layers (Fig. 7a). After printing, the dissolution of GalC6 or GalC7 hydrogels is inspected visually and has been reported in Table 4. The formation of empty channels under the GalC9 top layers is checked. A 2.5% GalC6 hydrogel dissolved within 1h. Since printing the top layer of the structure required more than 20 minutes, this rate of the sacrificial layer dissolution is too fast. To slow-down the dissolution rate, GalC6 with a higher concentration has been used (5 wt%). The complete dissolution then occurred after 5 days. As far as GalC7 is concerned, at 2.5% no significant change had been observed for 7 days in 25 mL of water, thus the amount of water was doubled to 50 mL. The gel finally dissolved after another week in 50 mL of water. GalC8 hydrogels slowly and partly dissolves within 14 days in 25 mL of water. A thin layer of gel is persistent over months. Finally, GalC9 hydrogels did not dissolve after several months and thus have been considered as persistent gels. The final concentrations of the gelators printed in a 10 layers pattern in a bath of 25 mL have been calculated and compared to the solubilities (Table 4). For GalC6, GalC7 and GalC8, these concentrations are always lower than the solubility measured by NMR. It explains the solubilization of the structures with time and confirms that they can be used as sacrificial inks. Conversely, the final concentration of GalC9 is higher than its solubility, which explains that it does not dissolves, confirming that is can be used as a persistent ink. To avoid dissolution, it is possible to remove a large volume of water after printing. A large volume of water is used to ensure the quick dilution of DMSO, so that it would not modify too much the properties of the coagulation bath. But after printing, this large volume can be removed to preserve the structures from further dissolution. Fig. 7b-d shows that empty channels have been successfully formed after the dissolution of the GalC7 sacrificial hydrogel. The different printed gels can be imbricated properly. Extra examples are given in SI-5. It means that GalC7 or GalC6 hydrogels can support the printing of top layers of GalC9. The GalC9 solution does not diffuse within the sacrificial hydrogels during the printing process: it would have led to some filling of the channels with GalC9. Also, the printed GalC9 gel is stiff and cohesive enough to not collapse nor bend under its own weight after the dissolution of layers below. It is stiff and cohesive despite its supramolecular microstructure made of micrometric flakes. The resulting patterns made of GalC9 with the channels are kept unchanged after several months in the water bath. To better image the interlocking of the hydrogels, the nested structure has been printed also with green and red fluorospheres. The structure is still well-defined but charging the ink with fluorospheres tends to make the hydrogel more brittle (Fig. 7e). It dissociates easily when the bath is moved.

Table 4. Dissolution rates of 3D-printed hydrogels of GalC6. GalC7 and GalC8 imbricated with a 3D printed GalC9 hydrogel. Final concentrations of N-hexyl, N-heptyl, N-nonyl-D-galactonamides (resp. GalC6, GalC7, GalC9) in the 25mL water bath after printing 10 layers of the imbricated structures.

Gelators	GalC6		GalC7		GalC8 (*)	GalC9
Concentration (% w/v)	2.5	5	1	2.5	1	1
Number of layers	10	20	60	10	10	20
Time required to completely dissolve the layers of gel (visual inspection)	1h	5 days	7 days	7 days in 25 mL + 7 days in 50 mL	Partly dissolved until saturation of the bath in the first days. then unchanged over 14 days	No significant changes over 1 month
Volume of gel injected in 25mL of water (µL)		10.3	9.2	10.3	10.6	112.69
Final concentrations of gelators in 25 mL of water (µmol/mL)		0.074	0.013	0.035	0.014	0.14
Solubility in D_2O measured by NMR (from Table 3) (µmol/mL)	5.3		1.2		0.3	0.07

* For GalC8 the values are given for a "F" pattern (not for an imbricated pattern)

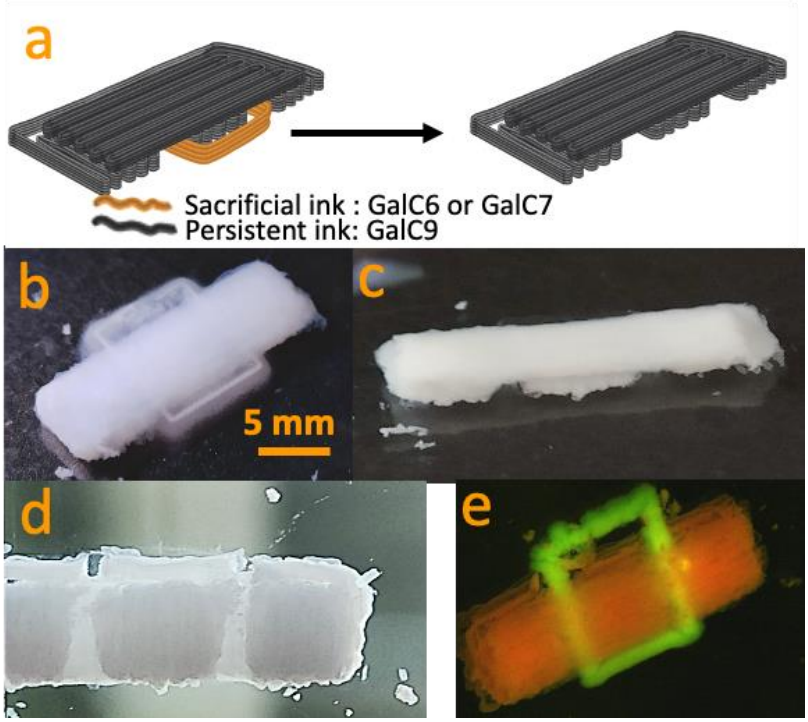

Fig. 7. (a) 3D printing pattern and sequence; (b) Imbricated gel structure just after printing (top view) (base and top rectangle are made of GalC9, the sacrificial square is made of GalC7). (c,d) 3D printed structure after complete dissolution of GalC7 after 7 days (c: side view and d: bottom view). (e) Imbrication of a GalC9 gel with red fluorospheres and a GalC7 gel with green fluorospheres.

6- Human Mesenchymal stem cell culture on GalC9 hydrogels

In our previous study, we have shown that cell culture of human neural stem cells was possible on N-heptyl-D-galactonamide (GalC7) hydrogels prepared by slow cooling of a hot aqueous solution of this gelator into culture wells. The gel sets upon cooling. However, after 7 days, the amount of remaining gel was very low. To stabilize the culture before immunostaining and to avoid washing out the cells, it was necessary to embed the whole culture in a transparent acrylamide hydrogel. When GalC7 hydrogels are prepared by wet spinning (with a solvent exchange method similar to the 3D printing method), cell culture was possible during 2 days only. The gels were too fragile, notably because the supramolecular fibers formed in these conditions are much thinner (≈140 nm width) compared with the fibers of gels prepared by cooling (≈0.5 to 35 µm width). We also reasoned on solubility data, which show that GalC7 can be solubilized in a large amount of water, explaining the gel fragility. By lengthening the alkyl chain, we obtained a less soluble gelator, the N-nonyl-D-galactonamide GalC9. We started to explore the suitability of GalC9 gels prepared with both methods. 3D printed hydrogels are first printed in wells filled with water (Fig. SI 6a). Then hydrogels obtained by heating-cooling are prepared in vials and transferred in the wells. All wells are rinsed progressively with PBS to remove water and/or DMSO. These rinsing steps do not change the macroscopic aspect of gels prepared by cooling. They kept a very good cohesion before and after PBS rinsing which is related to the fibrillar microstructure (Fig. 8e). No fragment nor isolated bundles of fibers can be seen around the gel (Fig. 8d, blue frames). Besides, 3D printed hydrogels disintegrate in part when water is replaced by PBS (Fig. 8d, brown frames). Fragments dissociates in the periphery of the printed structure, but a cohesive core remained. This fragility is related to the microstructure. As seen in Fig 6d, the gel has lost the fibrillar structure and is made of flakes.

Human mesenchymal stem cells derived from adipose tissue are seeded on GalC9 hydrogels prepared by cooling or by 3D printing. After 7 days of culture, a live dead assay is performed. On the gels prepared by cooling, numerous elongated live cells are observed (Fig. 8e and SI 6c). It shows that the cells have adhered to the gel and that the gel is suitable for cell culture. The volume of gel is still very large after 7 days (Fig. 8c, blue frames), contrary to what has been observed in a previous work with GalC7 hydrogels [9]. This has been ascribed to the much lower solubility of GalC9 compared with GalC7. Conversely, 3D printed gels are not cohesive enough to withstand cell growth for 7 days (Fig. 8a,b,c, brown frames). It impaired a complete analysis of the cell culture on 3D-printed hydrogels. Some cells found on these fragments are alive but they are rather round (Fig. 8f). Short extensions are sometimes observed. Both hydrogel fibers are composed of only GalC9 molecules.

The difference between the two modes of preparation lies in the microstructure of the gel fibers and the possible residual amount of DMSO in 3D printed hydrogels. However, 3D-printed gels have been extensively rinsed to remove DMSO. The calculated residual concentration is below 0.2 µL/mL. At such a concentration, strong deleterious effects on cells are not expected [60,61]. Thus, we make the hypothesis that difference of cell behavior would be merely related to the microstructure. In gels prepared by cooling, the microstructure is made of large and long flat ribbons, some being larger than 10 µm. In 3D printed gels, it is made of short micrometric flakes explaining that this gel is less cohesive. At the microscopic level, the mechanical properties of these two gels are probably very different and could have a significant effect on the cell culture stability.

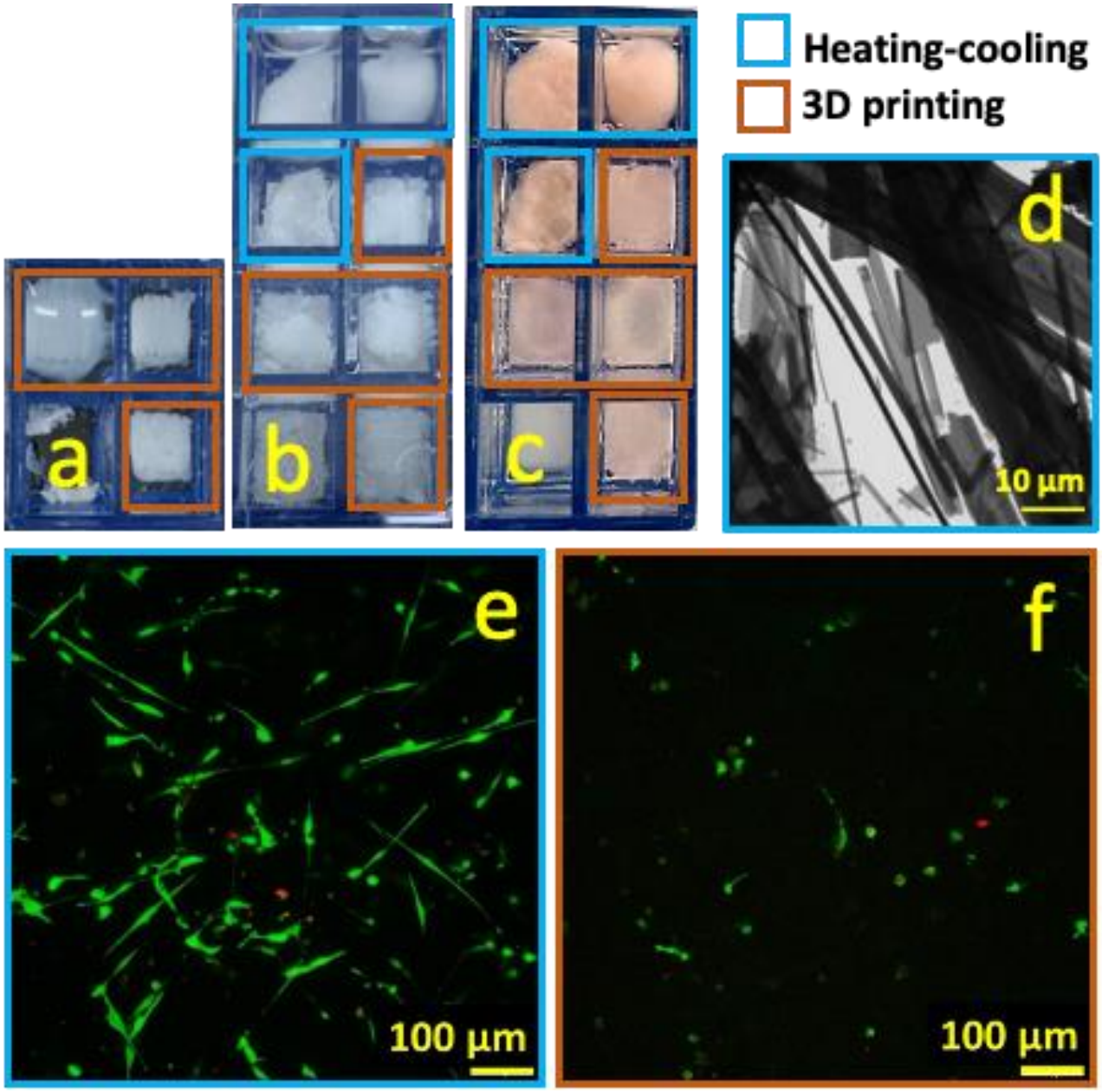

Fig. 8. Cell culture assay with human mesenchymal stem cells on N-nonyl-D-galactonamide hydrogel (GalC9). Aspect of GalC9 hydrogel in the 8 well chambers slide prepared by cooling a hot solution (blue frames) or by 3D printing (brown frames): (a) after 3D printing in water; (b) after rinsing with PBS; (c) after 7 days of culture. (d) Transmission Electron Microscopy of N-nonyl-D-galactonamide hydrogel prepared by cooling (Electron microscopy of 3D printed gels are in Fig. 6). (e,f) Live-dead assays of hMSC after 7 days of culture on a N-nonyl-D-galactonamide hydrogel GalC9 (e) prepared by cooling (f) prepared by 3D printing.

Conclusion

In this work, we showed that carbohydrate molecular hydrogels of N-alkyl-D-galactonamides can be 3D printed by a solvent exchange method. The principle has been shown precedingly with N-heptyl-D-galactonamide, but the resulting printed gels were quite soluble in water (1.2 µmol/mL) and too fragile to sustain cell culture [15,41]. To solve this problem, we extended the method to more hydrophobic gelators, such as N-nonyl-D-galactonamide, which solubility in water is much lower (0.07 µmol/mL). Imbricated constructions with N-hexyl or N-heptyl-D-galactonamides as sacrificial

inks and N-nonyl-D-galactonamide as non-soluble ink have been made. After the dissolution of the N-hexyl or N-heptyl-D-galactonamide hydrogels, free-standing and persistent structures of N-nonyl-D-galactonamide hydrogel with empty channels are obtained.

Concerning cell culture, human mesenchymal stem cells developed well on N-nonyl-D-galactonamide hydrogels prepared by cooling a hot aqueous solution of the gelator. The gel is highly cohesive and fibrous. It is still cohesive and not visually degraded after 7 days of culture. It is a strong improvement compared with hydrogels of N-heptyl-D-galactonamide used in our previous work. On the latter, the cell culture was limited to 7 to 10 days, because the gel was nearly completely eliminated after this time [9]. This comparison shows that lengthening the alkyl chain is thus a good strategy to increase the durability of these molecular gels. Conversely, on 3D-printed hydrogels of N-nonyl-D-galactonamide the cell development is not good. These 3D printed gels are made of an assembly of self-assembled flakes instead of long fibers. This microstructure makes these hydrogels friable which precludes cell culture and a complete analysis of the samples. Since the chemical composition of the scaffolds is the same in both conditions (only made of N-nonyl-D-galactonamide), these results also showed that the cell fate is probably affected primarily by the microstructure of the gel.

Thus, in this work, the stability of the 3D printed gels has been improved thanks to the use of gelators of low solubility. But this stability has been gained to the detriment of the fibrillar structure, leading to friable gels. The decrease of supramolecular fiber length is linked to the decrease of solubility during the self-assembling process [56,57]. Thus, a next improvement would be to find 3D printing conditions in which the solubility is high enough all along this process. We expect it would give molecular hydrogels of low solubility with a fibrillar structure and a good mechanical strength, making them suitable for cell culture.

Beyond applications to cell culture scaffolds, the 3D printing method developed here show that it is possible to get free-standing hydrogels made by 3D printing without any polymer. This strategy can be extended to molecular gels with other chemical structures [16,40]. It could be extended also to inorganic colloidal species. These species must be able to percolate under solvent exchange conditions or at the interface between two miscible solvents [62]. Gels of inorganic nanoparticles used to prepare aerogels may be adapted to this technique [63]. They could give interesting architectures is coupled to the present 3D printing method. Finally, by taking the adequate gelator, the structure dissolves spontaneously with time. The gel could be used as a vehicle to print other compounds before eliminating the scaffold by simple dissolution. Implementation of co-extrusion methods [64] and printing in colloidal baths to improve resolution [65] could further extend the scope of this technique.

Acknowledgments

Jean-Michel Martin (ICT, Institut de Chimie de Toulouse, Electronic facilities) and Salomé Peters (Internship from Ecole Nationale Vétérinaire de Toulouse, ENVT) are acknowledged for the preliminary experiments that were undertaken to design and to select an affordable 3D printing equipment for this liquid/liquid ink/coagulation bath system. C. Toppan (ICT) is acknowledged for NMR facilities. The CMEAB (Centre de Microscopie Electronique Appliqué à la Biologie) is acknowledged for TEM and cryo-TEM experiments. Anaïs Chalard is acknowledged for the extra image of cryo-SEM of a 3D printed GalC7 hydrogel to compare with the present 3D printed hydrogels (Fig. 6b). This image is extracted for a preceding work already published in ref [15]. This work was supported by the French National Research Agency (Agence Nationale de la Recherche) (D.B.'s grant and financial support, ANR "Neuraxe", grant N°ANR-15-CE07-0007-01) and the French Ministry of

Higher Education, Research and Innovation (Ministère de l'Enseignement Supérieur, de la Recherche et de l'Innovation) for F.A.'s grant.

Supporting Material

Supplementary images of the printed patterns in different conditions; scheme of 22 positions on the pattern; width vs extrusion rate graphs; NMR and MS spectra of N-alkyl-D-galactonamides after heating, cell culture assays images.

References

[1] T. Saydé, O. El Hamoui, B. Alies, K. Gaudin, G. Lespes, S. Battu, Biomaterials for Three-Dimensional Cell Culture: From Applications in Oncology to Nanotechnology, Nanomaterials (Basel). 11 (2021) 481. https://doi.org/10.3390/nano11020481.
[2] G. Bouguéon, T. Kauss, B. Dessane, P. Barthélémy, S. Crauste-Manciet, Micro- and nano-formulations for bioprinting and additive manufacturing, Drug Discovery Today. 24 (2019) 163–178. https://doi.org/10.1016/j.drudis.2018.10.013.
[3] C. Mota, S. Camarero-Espinosa, M.B. Baker, P. Wieringa, L. Moroni, Bioprinting: From Tissue and Organ Development to in Vitro Models, Chem. Rev. 120 (2020) 10547–10607. https://doi.org/10.1021/acs.chemrev.9b00789.
[4] J. Chen, D. Huang, L. Wang, J. Hou, H. Zhang, Y. Li, S. Zhong, Y. Wang, Y. Wu, W. Huang, 3D bioprinted multiscale composite scaffolds based on gelatin methacryloyl (GelMA)/chitosan microspheres as a modular bioink for enhancing 3D neurite outgrowth and elongation, Journal of Colloid and Interface Science. 574 (2020) 162–173. https://doi.org/10.1016/j.jcis.2020.04.040.
[5] J. Li, C. Wu, P.K. Chu, M. Gelinsky, 3D printing of hydrogels: Rational design strategies and emerging biomedical applications, Materials Science and Engineering: R: Reports. 140 (2020) 100543. https://doi.org/10.1016/j.mser.2020.100543.
[6] E.R. Draper, D.J. Adams, Controlling the Assembly and Properties of Low-Molecular-Weight Hydrogelators, Langmuir. 35 (2019) 6506–6521. https://doi.org/10.1021/acs.langmuir.9b00716.
[7] O. Chaudhuri, L. Gu, D. Klumpers, M. Darnell, S.A. Bencherif, J.C. Weaver, N. Huebsch, H. Lee, E. Lippens, G.N. Duda, D.J. Mooney, Hydrogels with tunable stress relaxation regulate stem cell fate and activity, Nature Materials. 15 (2016) 326–334. https://doi.org/10.1038/nmat4489.
[8] C.M. Madl, B.L. LeSavage, R.E. Dewi, C.B. Dinh, R.S. Stowers, M. Khariton, K.J. Lampe, D. Nguyen, O. Chaudhuri, A. Enejder, S.C. Heilshorn, Maintenance of neural progenitor cell stemness in 3D hydrogels requires matrix remodelling, Nature Mater. 16 (2017) 1233–1242. https://doi.org/10.1038/nmat5020.
[9] A. Chalard, L. Vaysse, P. Joseph, L. Malaquin, S. Souleille, B. Lonetti, J.-C. Sol, I. Loubinoux, J. Fitremann, Simple Synthetic Molecular Hydrogels from Self-Assembling Alkylgalactonamides as Scaffold for 3D Neuronal Cell Growth, ACS Appl. Mater. Interfaces. 10 (2018) 17004–17017. https://doi.org/10.1021/acsami.8b01365.
[10] E.J. Berns, S. Sur, L. Pan, J.E. Goldberger, S. Suresh, S. Zhang, J.A. Kessler, S.I. Stupp, Aligned neurite outgrowth and directed cell migration in self-assembled monodomain gels, Biomaterials. 35 (2014) 185–195. https://doi.org/10.1016/j.biomaterials.2013.09.077.
[11] L. Latxague, S. Benizri, A. Gaubert, J. Tolchard, D. Martinez, E. Morvan, A. Grélard, A. Saad, B. Habenstein, A. Loquet, P. Barthélémy, Bolaamphiphile-based supramolecular gels with drugs eliciting membrane effects, Journal of Colloid and Interface Science. 594 (2021) 857–863.

https://doi.org/10.1016/j.jcis.2021.03.026.
[12] T. Maruyama, W.K. Restu, Intracellular self-assembly of supramolecular gelators to selectively kill cells of interest, Polymer Journal. 52 (2020) 883–889. https://doi.org/10.1038/s41428-020-0335-8.
[13] S. Almohammed, M. Alruwaili, E.G. Reynaud, G. Redmond, J.H. Rice, B.J. Rodriguez, 3D-Printed Peptide-Hydrogel Nanoparticle Composites for Surface-Enhanced Raman Spectroscopy Sensing, ACS Appl. Nano Mater. 2 (2019) 5029–5034. https://doi.org/10.1021/acsanm.9b00940.
[14] B. Dessane, R. Smirani, G. Bouguéon, T. Kauss, E. Ribot, R. Devillard, P. Barthélémy, A. Naveau, S. Crauste-Manciet, Nucleotide lipid-based hydrogel as a new biomaterial ink for biofabrication, Scientific Reports. 10 (2020) 2850. https://doi.org/10.1038/s41598-020-59632-w.
[15] A. Chalard, M. Mauduit, S. Souleille, P. Joseph, L. Malaquin, J. Fitremann, 3D printing of a biocompatible low molecular weight supramolecular hydrogel by dimethylsulfoxide water solvent exchange, Additive Manufacturing. 33 (2020) 101162. https://doi.org/10.1016/j.addma.2020.101162.
[16] C.C. Piras, A.G. Kay, P.G. Genever, J. Fitremann, D.K. Smith, Self-assembled gel tubes, filaments and 3D-printing with in situ metal nanoparticle formation and enhanced stem cell growth, Chem. Sci. (2022). https://doi.org/10.1039/D1SC06062G.
[17] H. Yang, S. Zhang, K. Liu, Y. Fang, Calix[4]arene-based low molecular mass gelators to form gels in organoalkoxysilanes, RSC Adv. 6 (2016) 109969–109977. https://doi.org/10.1039/C6RA22731G.
[18] B. Raphael, T. Khalil, V.L. Workman, A. Smith, C.P. Brown, C. Streuli, A. Saiani, M. Domingos, 3D cell bioprinting of self-assembling peptide-based hydrogels, Materials Letters. 190 (2017) 103–106. https://doi.org/10.1016/j.matlet.2016.12.127.
[19] M.C. Nolan, A.M.F. Caparrós, B. Dietrich, M. Barrow, E.R. Cross, M. Bleuel, S.M. King, D.J. Adams, Optimising low molecular weight hydrogels for automated 3D printing, Soft Matter. 13 (2017) 8426–8432. https://doi.org/10.1039/C7SM01694H.
[20] F. Gelain, Z. Luo, S. Zhang, Self-Assembling Peptide EAK16 and RADA16 Nanofiber Scaffold Hydrogel, Chem. Rev. 120 (2020) 13434–13460. https://doi.org/10.1021/acs.chemrev.0c00690.
[21] H. Jian, M. Wang, Q. Dong, J. Li, A. Wang, X. Li, P. Ren, S. Bai, Dipeptide Self-Assembled Hydrogels with Tunable Mechanical Properties and Degradability for 3D Bioprinting, ACS Appl. Mater. Interfaces. 11 (2019) 46419–46426. https://doi.org/10.1021/acsami.9b13905.
[22] H.H. Susapto, D. Alhattab, S. Abdelrahman, Z. Khan, S. Alshehri, K. Kahin, R. Ge, M. Moretti, A.-H. Emwas, C.A.E. Hauser, Ultrashort Peptide Bioinks Support Automated Printing of Large-Scale Constructs Assuring Long-Term Survival of Printed Tissue Constructs, Nano Lett. 21 (2021) 2719–2729. https://doi.org/10.1021/acs.nanolett.0c04426.
[23] S. Rauf, H.H. Susapto, K. Kahin, S. Alshehri, S. Abdelrahman, J.H. Lam, S. Asad, S. Jadhav, D. Sundaramurthi, X. Gao, C.A.E. Hauser, Self-assembling tetrameric peptides allow in situ 3D bioprinting under physiological conditions, J. Mater. Chem. B. 9 (2021) 1069–1081. https://doi.org/10.1039/D0TB02424D.
[24] A.M. Fuentes-Caparrós, Z. Canales-Galarza, M. Barrow, B. Dietrich, J. Läuger, M. Nemeth, E.R. Draper, D.J. Adams, Mechanical Characterization of Multilayered Hydrogels: A Rheological Study for 3D-Printed Systems, Biomacromolecules. 22 (2021) 1625–1638. https://doi.org/10.1021/acs.biomac.1c00078.
[25] N.A. Sather, H. Sai, I.R. Sasselli, K. Sato, W. Ji, C.V. Synatschke, R.T. Zambrotta, J.F. Edelbrock, R.R. Kohlmeyer, J.O. Hardin, J.D. Berrigan, M.F. Durstock, P. Mirau, S.I. Stupp, 3D Printing of Supramolecular Polymer Hydrogels with Hierarchical Structure, Small. 17 (2021) 2005743. https://doi.org/10.1002/smll.202005743.
[26] C. Zheng, S. Lin, C. Hu, Y. Li, B. Li, Y. Yang, Chirality-driven molecular packing structure difference and potential application for 3D printing of a series of bola-type Ala–Phe dipeptides, New

J. Chem. 44 (2020) 20726–20733. https://doi.org/10.1039/D0NJ04745G.
[27] Y. Xia, B. Xue, M. Qin, Y. Cao, Y. Li, W. Wang, Printable Fluorescent Hydrogels Based on Self-Assembling Peptides, Scientific Reports. 7 (2017). https://doi.org/10.1038/s41598-017-10162-y.
[28] A.T.L. Tan, S. Nagelberg, E. Chang-Davidson, J. Tan, J.K.W. Yang, M. Kolle, A.J. Hart, In-Plane Direct-Write Assembly of Iridescent Colloidal Crystals, Small. 16 (2020) 1905519. https://doi.org/10.1002/smll.201905519.
[29] S. Kyle, Z.M. Jessop, A. Al-Sabah, I.S. Whitaker, 'Printability' of Candidate Biomaterials for Extrusion Based 3D Printing: State-of-the-Art, Advanced Healthcare Materials. 6 (2017) 1700264. https://doi.org/10.1002/adhm.201700264.
[30] A. Schwab, R. Levato, M. D'Este, S. Piluso, D. Eglin, J. Malda, Printability and Shape Fidelity of Bioinks in 3D Bioprinting, Chem. Rev. 120 (2020) 11028–11055. https://doi.org/10.1021/acs.chemrev.0c00084.
[31] J. Yang, M. Chen, H. Lee, Z. Xu, Z. Zhou, S.-P. Feng, J.T. Kim, Three-Dimensional Printing of Self-Assembled Dipeptides, ACS Appl. Mater. Interfaces. 13 (2021) 20573–20580. https://doi.org/10.1021/acsami.1c03062.
[32] Q. Tang, T.N. Plank, T. Zhu, H. Yu, Z. Ge, Q. Li, L. Li, J.T. Davis, H. Pei, Self-Assembly of Metallo-Nucleoside Hydrogels for Injectable Materials That Promote Wound Closure, ACS Appl. Mater. Interfaces. 11 (2019) 19743–19750. https://doi.org/10.1021/acsami.9b02265.
[33] A. Biswas, S. Malferrari, D. M. Kalaskar, A. K. Das, Arylboronate esters mediated self-healable and biocompatible dynamic G-quadruplex hydrogels as promising 3D-bioinks, Chemical Communications. 54 (2018) 1778–1781. https://doi.org/10.1039/C7CC09051J.
[34] Q. Qin, F. Yang, X. Zhang, T. Shi, Y. Shao, H. Sun, C. Chen, J. Hao, Z. Guo, 3D printing of tantalum parts based on low molecular mass organic gel system, International Journal of Refractory Metals and Hard Materials. 84 (2019) 105014. https://doi.org/10.1016/j.ijrmhm.2019.105014.
[35] K. Liu, S. Zang, R. Xue, J. Yang, L. Wang, J. Huang, Y. Yan, Coordination-Triggered Hierarchical Folate/Zinc Supramolecular Hydrogels Leading to Printable Biomaterials, ACS Appl. Mater. Interfaces. 10 (2018) 4530–4539. https://doi.org/10.1021/acsami.7b18155.
[36] Z. Zhou, M. Samperi, L. Santu, G. Dizon, S. Aboarkaba, D. Limón, C. Tuck, L. Pérez-García, D.J. Irvine, D.B. Amabilino, R. Wildman, An imidazolium-based supramolecular gelator enhancing interlayer adhesion in 3D printed dual network hydrogels, Materials & Design. 206 (2021) 109792. https://doi.org/10.1016/j.matdes.2021.109792.
[37] Q. Wei, W. Xu, M. Liu, Q. Wu, L. Cheng, Q. Wang, Viscosity-controlled printing of supramolecular-polymeric hydrogels via dual-enzyme catalysis, J. Mater. Chem. B. 4 (2016) 6302–6306. https://doi.org/10.1039/C6TB01792D.
[38] C. Cofiño, S. Perez-Amodio, C.E. Semino, E. Engel, M.A. Mateos-Timoneda, Development of a Self-Assembled Peptide/Methylcellulose-Based Bioink for 3D Bioprinting, Macromol. Mater. Eng. 304 (2019) 1900353. https://doi.org/10.1002/mame.201900353.
[39] P.R.A. Chivers, D.K. Smith, Shaping and structuring supramolecular gels, Nature Reviews Materials. 4 (2019) 463–478. https://doi.org/10.1038/s41578-019-0111-6.
[40] D. Bordignon, B. Lonetti, C. Coudret, P. Roblin, P. Joseph, L. Malaquin, A. Chalard, J. Fitremann, Wet spinning of a library of carbohydrate low molecular weight gels, Journal of Colloid and Interface Science. 603 (2021) 333–343. https://doi.org/10.1016/j.jcis.2021.06.058.
[41] A. Chalard, P. Joseph, S. Souleille, B. Lonetti, N. Saffon-Merceron, I. Loubinoux, L. Vaysse, L. Malaquin, J. Fitremann, Wet spinning and radial self-assembly of a carbohydrate low molecular weight gelator into well organized hydrogel filaments, Nanoscale. 11 (2019) 15043–15056. https://doi.org/10.1039/C9NR02727K.
[42] R. Kubota, M. Makuta, R. Suzuki, M. Ichikawa, M. Tanaka, I. Hamachi, Force generation by a propagating wave of supramolecular nanofibers, Nature Communications. 11 (2020) 3541. https://doi.org/10.1038/s41467-020-17394-z.

[43] L. Friedrich, M. Begley, In situ characterization of low-viscosity direct ink writing: Stability, wetting, and rotational flows, Journal of Colloid and Interface Science. 529 (2018) 599–609. https://doi.org/10.1016/j.jcis.2018.05.110.
[44] T.-S. Jang, H.-D. Jung, H.M. Pan, W.T. Han, S. Chen, J. Song, 3D printing of hydrogel composite systems: Recent advances in technology for tissue engineering, Int J Bioprint. 4 (2018). https://doi.org/10.18063/ijb.v4i1.126.
[45] Z. Pei, Q. Zhang, Q. Li, C. Ji, Y. Liu, K. Yang, K. Zhuo, W. Zhang, S. Sang, A fully 3D printed electronic skin with bionic high resolution and air permeable porous structure, Journal of Colloid and Interface Science. 602 (2021) 452–458. https://doi.org/10.1016/j.jcis.2021.06.041.
[46] B.F. Winhard, S. Haugg, R. Blick, G.A. Schneider, K.P. Furlan, Direct writing of colloidal suspensions onto inclined surfaces: Optimizing dispense volume for homogeneous structures, Journal of Colloid and Interface Science. 597 (2021) 137–148. https://doi.org/10.1016/j.jcis.2021.03.017.
[47] M. Ávalos, R. Babiano, P. Cintas, A. Gómez-Carretero, J.L. Jiménez, M. Lozano, A.L. Ortiz, J.C. Palacios, A. Pinazo, A Family of Hydrogels Based on Ureido-Linked Aminopolyol-Derived Amphiphiles and Bolaamphiphiles: Synthesis, Gelation under Thermal and Sonochemical Stimuli, and Mesomorphic Characterization, Chem. Eur. J. 14 (2008) 5656–5669. https://doi.org/10.1002/chem.200701897.
[48] J.H. Fuhrhop, P. Schnieder, E. Boekema, W. Helfrich, Lipid bilayer fibers from diastereomeric and enantiomeric N-octylaldonamides, Journal of the American Chemical Society. 110 (1988) 2861–2867.
[49] B. Pfannemüller, W. Welte, Amphiphilic properties of synthetic glycolipids based on amide linkages. I. Electron microscopic studies on aqueous gels, Chemistry and Physics of Lipids. 37 (1985) 227–240. https://doi.org/10.1016/0009-3084(85)90011-8.
[50] G.B. Messaoud, P.L. Griel, S. Prévost, D. Hermida-Merino, W. Soetaert, S.L.K.W. Roelants, C.V. Stevens, N. Baccile, Single-molecule lamellar hydrogels from bolaform microbial glucolipids, Soft Matter. 16 (2020) 2528–2539. https://doi.org/10.1039/C9SM02158B.
[51] J. Morris, J. Bietsch, K. Bashaw, G. Wang, Recently Developed Carbohydrate Based Gelators and Their Applications, Gels. 7 (2021) 24. https://doi.org/10.3390/gels7010024.
[52] J. Bietsch, M. Olson, G. Wang, Fine-Tuning of Molecular Structures to Generate Carbohydrate Based Super Gelators and Their Applications for Drug Delivery and Dye Absorption, Gels. 7 (2021) 134. https://doi.org/10.3390/gels7030134.
[53] Y. Loo, A. Lakshmanan, M. Ni, L.L. Toh, S. Wang, C.A.E. Hauser, Peptide Bioink: Self-Assembling Nanofibrous Scaffolds for Three-Dimensional Organotypic Cultures, Nano Lett. 15 (2015) 6919–6925. https://doi.org/10.1021/acs.nanolett.5b02859.
[54] H. Leménager, L.M.A. Fiévet, F. Guilloton, A. Naji, J.-G. Descamps, B. Chaput, N. Suganuma, J.-C. Pagès, L. Sensebé, A. Carrière, L. Casteilla, F. Deschaseaux, Cell immaturity and white/beige adipocyte potential of primary human adipose-derived stromal cells are restrained by culture-medium TGFβ1, Stem Cells. 38 (2020) 782–796. https://doi.org/10.1002/stem.3164.
[55] B. Payre, E. Gontier, A. Jarray, Y. Martinez, J. p. Laugier, A. Delalleau, B. m. Gaillard, I. Anselme, D. Goudounèche, I. Fourquaux, M. Hemati, V. Gerbaud, M. b. Delisle, C. Guilbeau-Frugier, A new HPF specimen carrier adapter for the use of high-pressure freezing with cryoscanning electron microscope: two applications: stearic acid organization in a hydroxypropyl methylcellulose matrix and mice myocardium, Journal of Microscopy. 271 (2018) 255–265. https://doi.org/10.1111/jmi.12713.
[56] X.Y. Liu, Gelation with Small Molecules: from Formation Mechanism to NanostructureArchitecture, in: Low Molecular Mass Gelator, Springer, Berlin, Heidelberg, 2005: pp. 1–37. https://doi.org/10.1007/b107170.
[57] Y. Lan, M.G. Corradini, X. Liu, T.E. May, F. Borondics, R.G. Weiss, M.A. Rogers, Comparing and Correlating Solubility Parameters Governing the Self-Assembly of Molecular Gels

Using 1,3:2,4-Dibenzylidene Sorbitol as the Gelator, Langmuir. 30 (2014) 14128–14142. https://doi.org/10.1021/la5008389.
[58] T. Ozawa, T. Asakawa, V.M. Garamus, A. Ohta, S. Miyagishi, Effect of D2O Solvent on the Micellization Behavior of 2-Hydroxy-1,1,2,3,3-pentahydroperfluoroundecyldiethyl- ammonium Halides, J. Oleo Sci. 54 (2005) 4.
[59] B. Escuder, M. LLusar, J.F. Miravet, Insight on the NMR Study of Supramolecular Gels and Its Application to Monitor Molecular Recognition on Self-Assembled Fibers, J. Org. Chem. 71 (2006) 7747–7752. https://doi.org/10.1021/jo0612731.
[60] R. Pal, M.K. Mamidi, A.K. Das, R. Bhonde, Diverse effects of dimethyl sulfoxide (DMSO) on the differentiation potential of human embryonic stem cells, Arch Toxicol. 86 (2012) 651–661. https://doi.org/10.1007/s00204-011-0782-2.
[61] M. Awan, I. Buriak, R. Fleck, B. Fuller, A. Goltsev, J. Kerby, M. Lowdell, P. Mericka, A. Petrenko, Y. Petrenko, O. Rogulska, A. Stolzing, G.N. Stacey, Dimethyl sulfoxide: a central player since the dawn of cryobiology, is efficacy balanced by toxicity?, Regenerative Medicine. 15 (2020) 1463–1491. https://doi.org/10.2217/rme-2019-0145.
[62] Y. Xi, R.S. Lankone, L.-P. Sung, Y. Liu, Tunable thermo-reversible bicontinuous nanoparticle gel driven by the binary solvent segregation, Nat Commun. 12 (2021) 910. https://doi.org/10.1038/s41467-020-20701-3.
[63] F. Matter, A.L. Luna, M. Niederberger, From colloidal dispersions to aerogels: How to master nanoparticle gelation, Nano Today. 30 (2020) 100827. https://doi.org/10.1016/j.nantod.2019.100827.
[64] M. Costantini, C. Colosi, W. Święszkowski, A. Barbetta, Co-axial wet-spinning in 3D bioprinting: state of the art and future perspective of microfluidic integration, Biofabrication. 11 (2018) 012001. https://doi.org/10.1088/1758-5090/aae605.
[65] W. Hua, K. Mitchell, L. Raymond, B. Godina, D. Zhao, W. Zhou, Y. Jin, Fluid Bath-Assisted 3D Printing for Biomedical Applications: From Pre- to Postprinting Stages, ACS Biomater. Sci. Eng. 7 (2021) 4736–4756. https://doi.org/10.1021/acsbiomaterials.1c00910.

Supporting Material

3D printing of biocompatible low molecular weight gels: imbricated structures with sacrificial and persistent N-alkyl-D-galactonamides

Faniry Andriamiseza [a], Delphine Bordignon [a], Bruno Payré [b], Juliette Fitremann [a] *

[a] Laboratoire des IMRCP, Université de Toulouse, CNRS UMR 5623, Université Toulouse III – Paul Sabatier
[b] Centre de Microscopie Electronique Appliquée à la Biologie (CMEAB), Faculté de Médecine Rangueil, Université de Toulouse III Paul Sabatier, Bâtiment A5, R.D.C., 133 Route de Narbonne, 31400 Toulouse, France

SI-1- Images of the patterns in different conditions of printing for one layer

Fig. SI-1.1: Images of one-layer hydrogels of N-hexyl-D-galactonamide (concentration 5 wt%, 50 mg/mL in DMSO), printed in different conditions of printing speed and extrusion rate

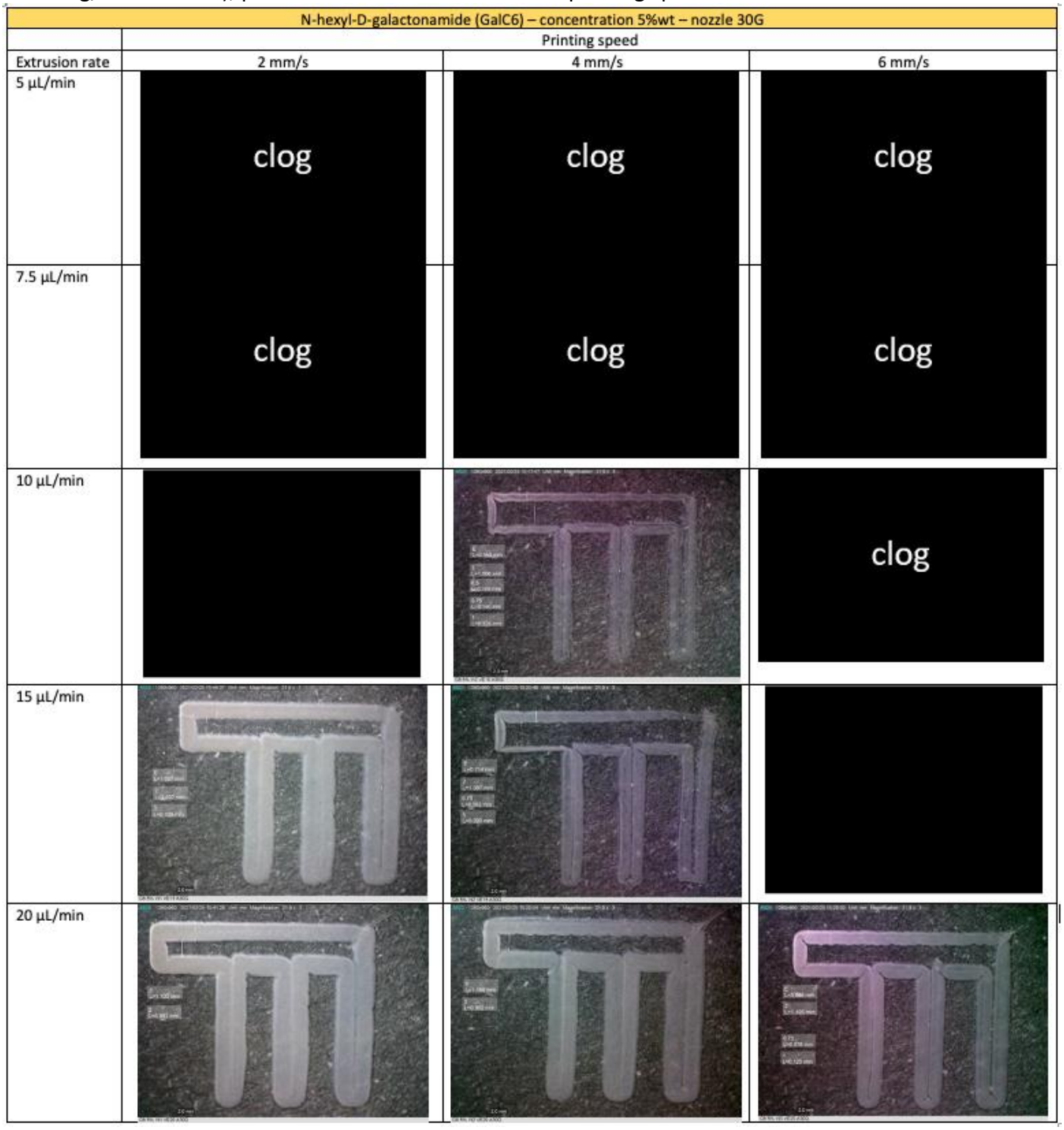

Fig. SI-1.2: Images of one-layer hydrogels of N-heptyl-D-galactonamide (concentration 2.5 wt%, 25 mg/mL in DMSO), printed in different conditions of printing speed and extrusion rate

N-heptyl-D-galactonamide (GalC7) – concentration 2.5%wt – nozzle 30G			
	Printing speed		
Extrusion rate	2 mm/s	4 mm/s	6 mm/s
5 µL/min	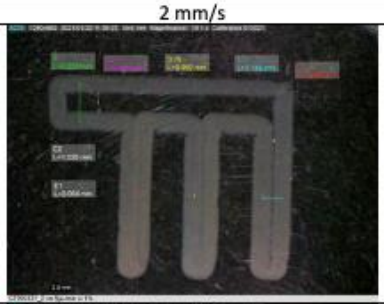	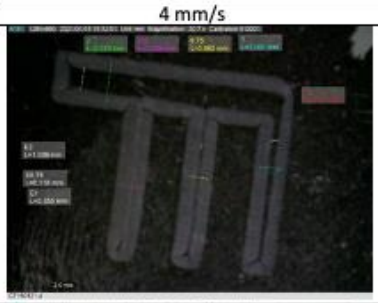	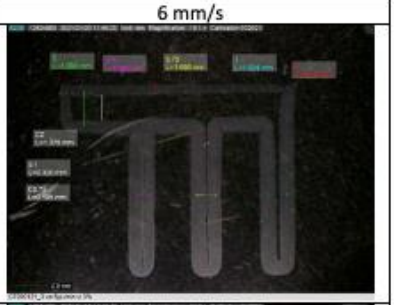
7.5 µL/min		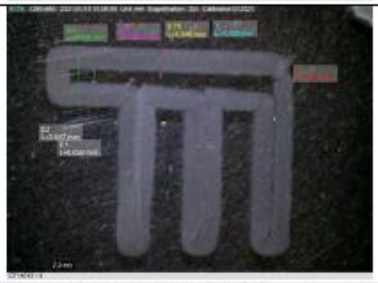	
10 µL/min		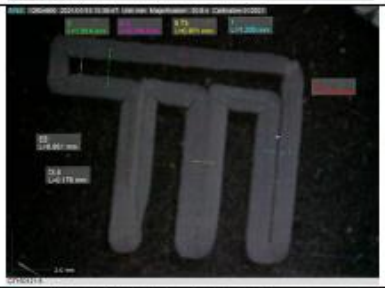	
15 µL/min		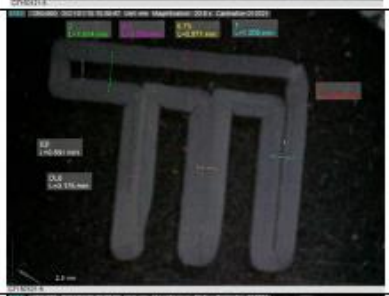	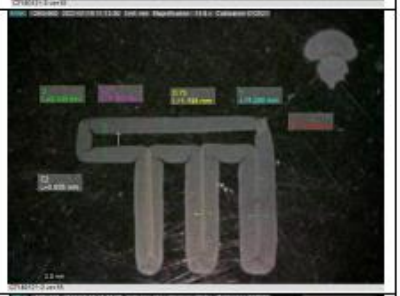
20 µL/min			

Fig. SI-1.3: Images of one-layer hydrogels of N-octyl-D-galactonamide (concentration 1 wt%, 10 mg/mL in DMSO), printed in different conditions of printing speed and extrusion rate

N-octyl-D-galactonamide (GalC8) – concentration 1%wt – nozzle 30G			
	Printing speed		
Extrusion rate	2 mm/s	4 mm/s	6 mm/s
5 µL/min	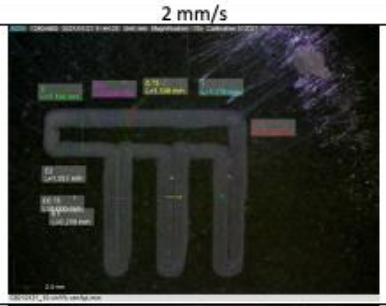	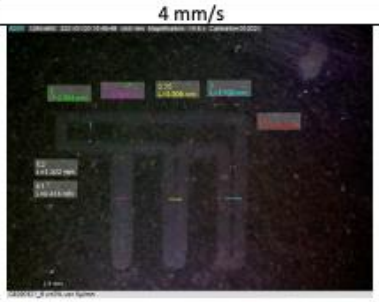	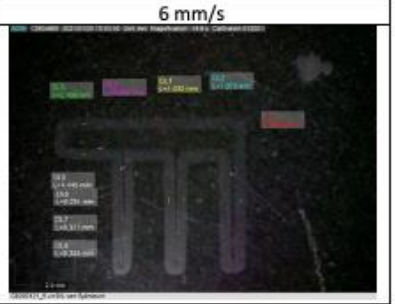
7.5 µL/min	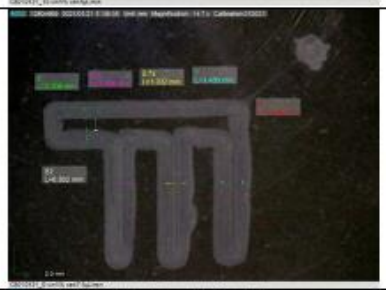	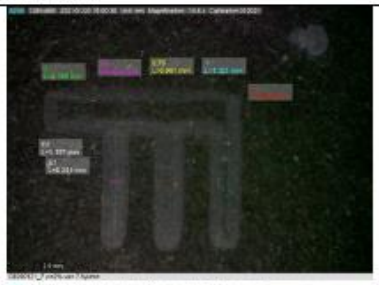	
10 µL/min			
15 µL/min	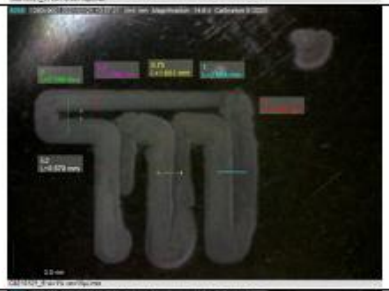		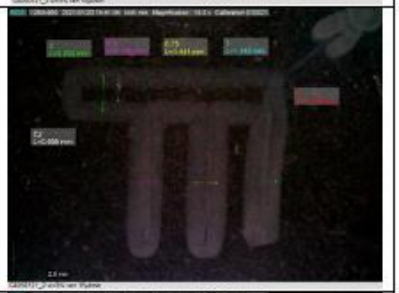
20 µL/min			

Fig. SI-1.4: Images of one-layer hydrogels of N-nonyl-D-galactonamide (concentration 1 wt%, 10 mg/mL in DMSO), printed in different conditions of printing speed and extrusion rate

N-nonyl-D-galactonamide (GalC9) – concentration 1%wt – nozzle 30G			
	Printing speed		
Extrusion rate	2 mm/s	4 mm/s	6 mm/s
5 µL/min	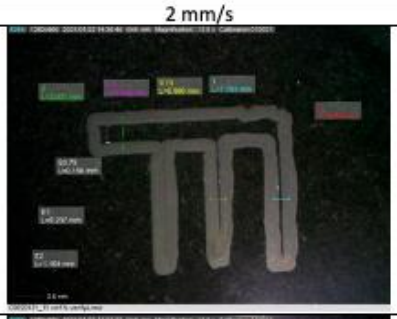	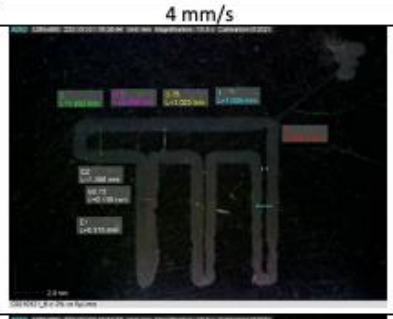	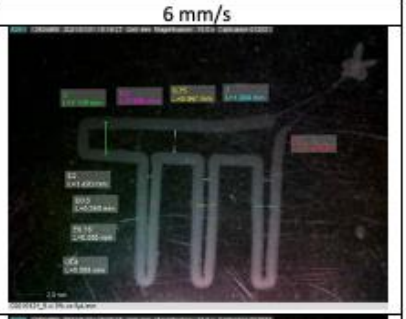
7.5 µL/min		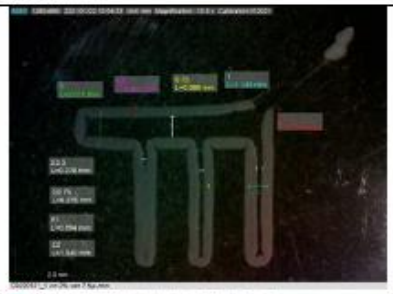	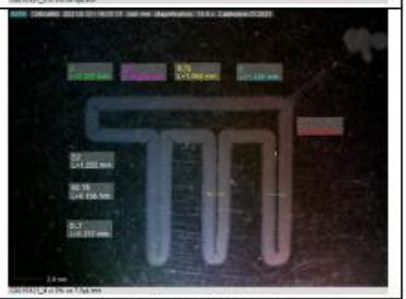
10 µL/min	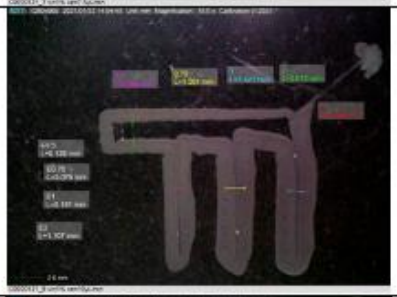	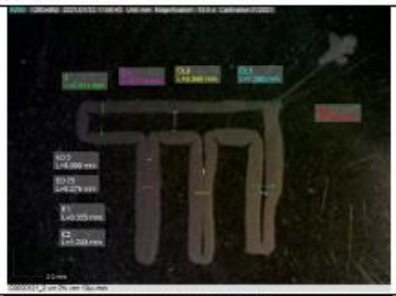	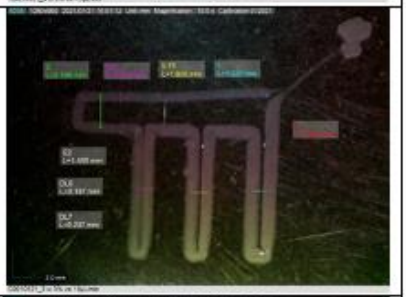
15 µL/min		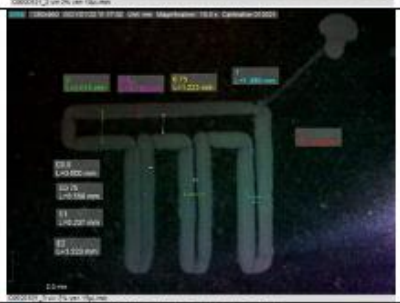	
20 µL/min	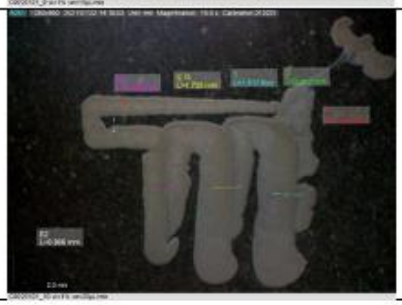	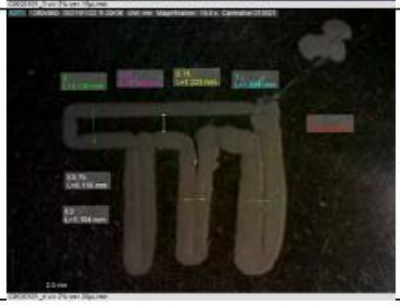	

SI-2 Best and worst patterns

Fig. SI-2.1. Selection of the thinnest width, the best resolution and the worst resolution respectively of GalC6 5 wt% at (a) 4mm/s and 10 µL/min; (b) 6mm/s and 20 µL/min; (c) 2mm/s and 20 µL/min.

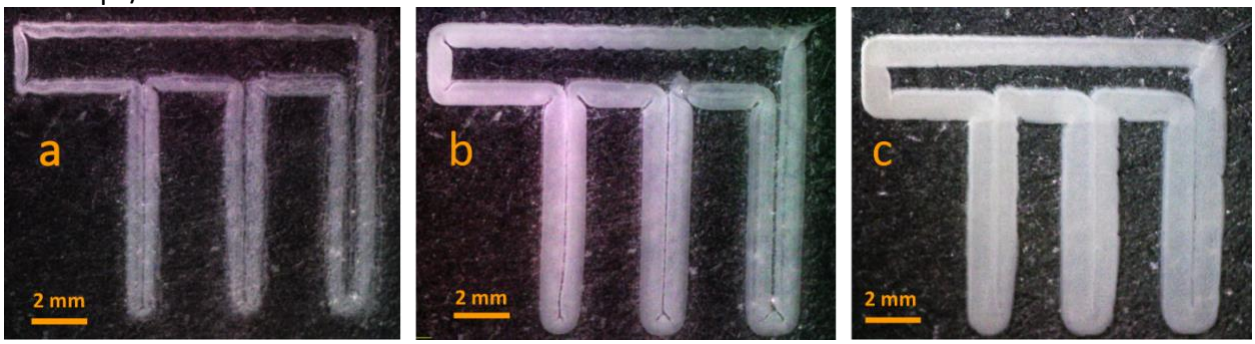

Fig. SI-2.2: Selection of the thinnest width, the best resolution and the worst resolution respectively of GalC7 2,5 wt% at (a) 4 mm/s and 5 µL/min; (b) 6 mm/s and 5 µL/min; (c) 2mm/s and 20 µL/min.

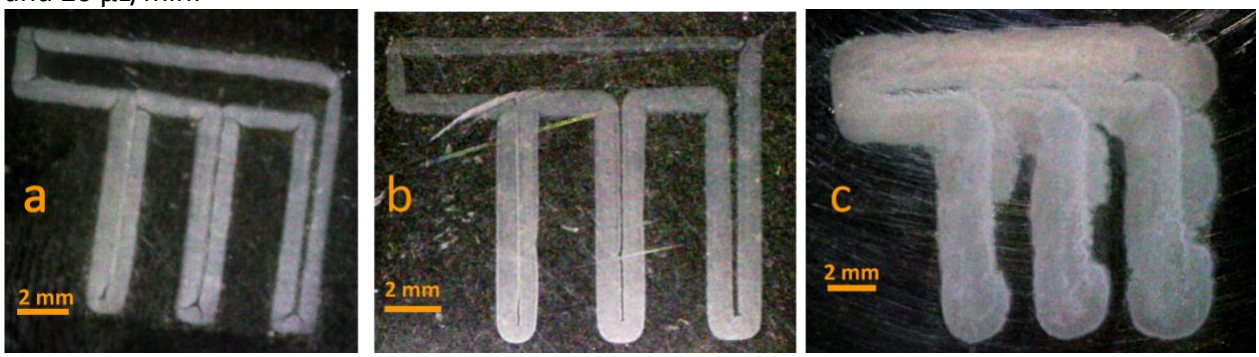

Fig. SI-2.3: Selection of the best and the worst resolution respectively of GalC8 (a) 6mm/s 5 µL/min (b) 2mm/s 20 µL/min

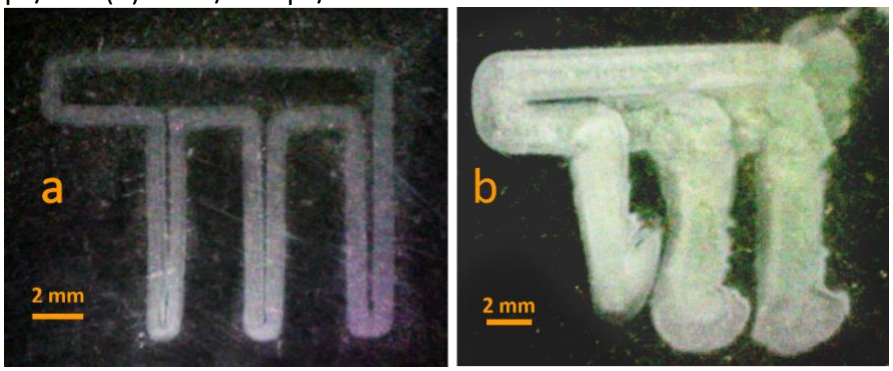

SI-3- Pattern positions and best resolution with GalC9 ink

Fig. SI-3.1: Scheme representing the “positions” of the 22 points of measurement.

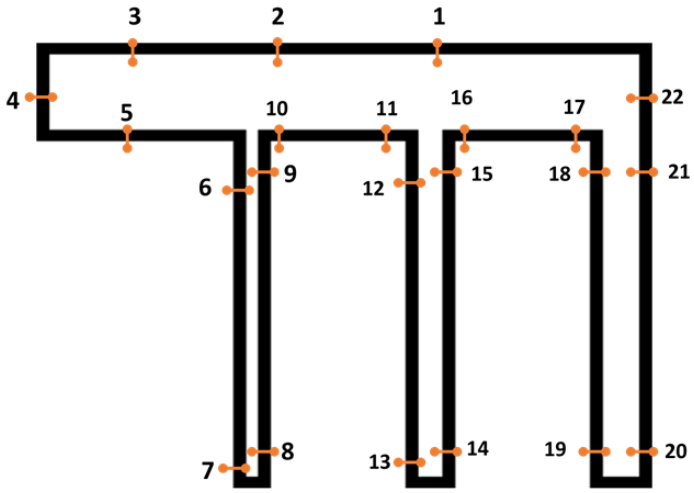

Fig. SI-3.2: Picture of a GalC9-printed pattern displaying the smallest width that could be obtained, and also the irregularity of the gel deposit width.

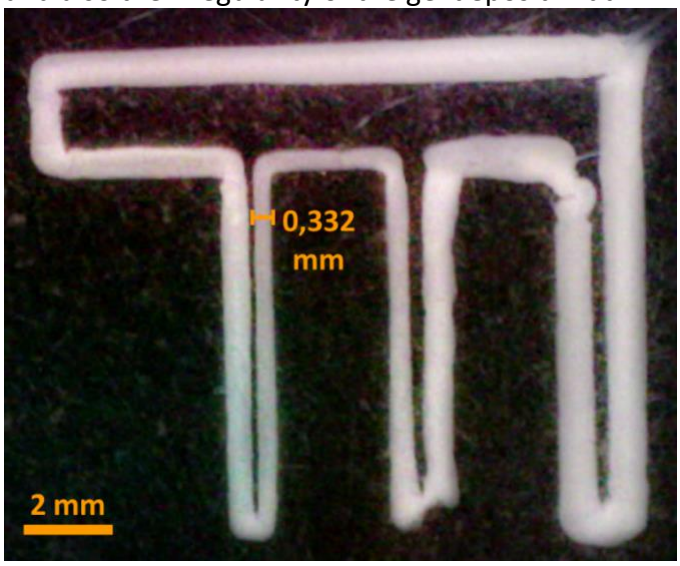

Fig. SI-3.3: Pattern width as a function of extrusion rate, at different printing speeds for GalC7 2.5 wt% ink

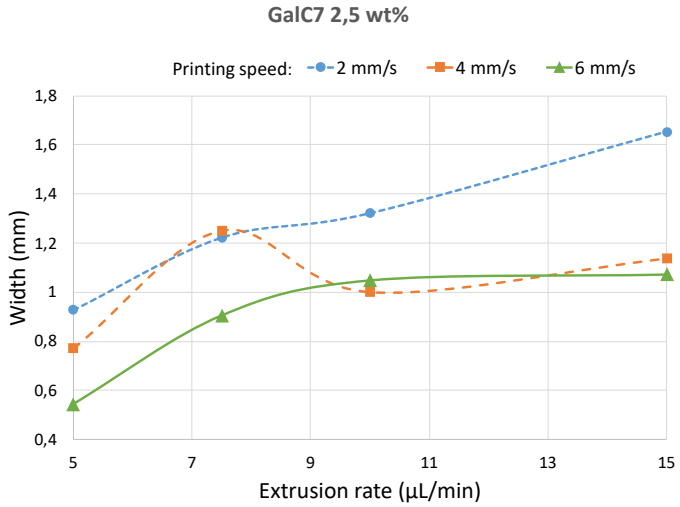

Fig. SI-3.4: Pattern width as a function of extrusion rate, at different printing speeds for GalC7 2.5 wt% ink

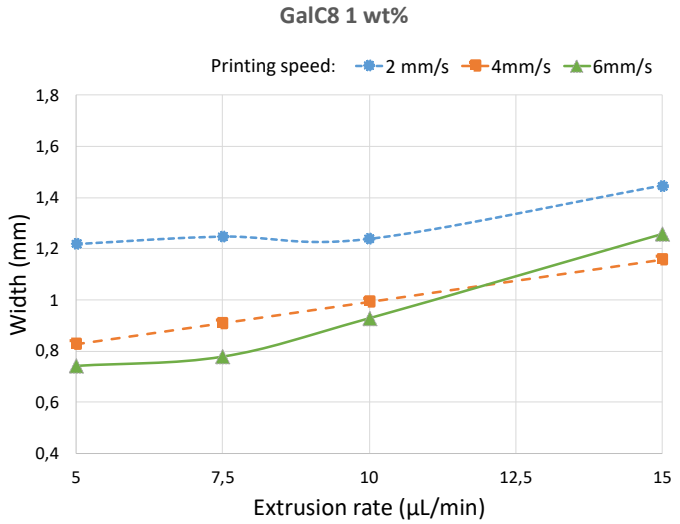

Fig. SI-3.5: Pattern width as a function of extrusion rate, at different printing speeds for GalC7 2.5 wt% ink

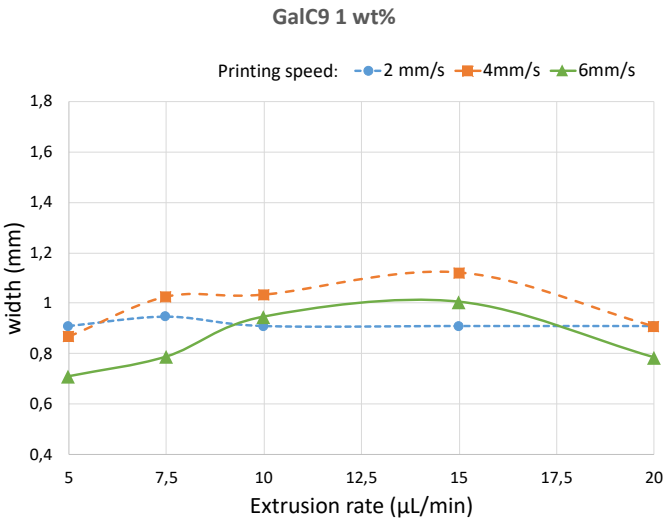

Table SI-3.6: Table of the occurrence of minimum and maximal width at each position

Range	Positions																					
	1	2	3	4	5	6	7	8	9	10	11	12	13	14	15	16	17	18	19	20	21	22
Min	12	1	2	1	2	0	1	9	9	0	0	0	0	3	3	3	0	0	0	3	1	1
2	2	5	1	3	2	0	2	12	7	0	1	0	0	7	5	0	1	0	1	1	1	0
3	4	7	3	2	4	3	5	4	2	0	1	1	0	7	4	0	1	0	0	1	1	1
4	2	4	4	6	4	0	1	3	1	5	1	0	0	8	4	1	0	0	1	3	2	1
5	3	3	7	3	1	1	2	5	4	1	1	2	2	4	3	0	1	2	0	4	2	0
6	5	2	3	6	2	4	4	6	4	4	1	0	2	2	1	1	0	0	0	4	0	0
7	0	1	1	6	6	1	1	3	6	4	1	0	0	6	5	1	2	0	0	4	2	1
8	5	2	2	4	3	7	1	2	3	1	1	1	2	1	5	0	0	1	0	1	7	2
9	1	4	5	2	4	5	6	1	0	0	1	0	3	2	2	3	2	3	1	3	2	1
10	0	4	4	3	8	8	1	2	2	1	1	0	3	3	1	0	0	0	2	4	2	2
11	1	2	3	3	1	3	8	1	2	3	4	3	5	1	1	1	3	1	1	1	3	0
12	2	1	2	1	5	2	1	1	0	8	1	5	2	2	1	3	2	4	2	4	1	1
13	2	5	4	1	4	4	2	0	2	1	0	3	3	1	2	3	3	1	2	2	3	3
14	2	2	1	4	2	3	1	0	1	3	4	2	2	1	0	6	3	5	0	1	7	1
15	1	0	1	1	0	3	1	0	2	7	3	9	5	1	6	1	0	5	2	2	0	1
16	2	2	1	0	0	2	2	1	0	1	5	4	5	0	2	4	3	6	6	2	1	2
17	1	3	2	1	1	2	4	0	1	3	5	4	3	0	2	5	1	2	2	5	1	3
18	0	0	2	1	0	0	1	0	3	2	4	2	4	2	1	5	2	9	4	0	5	4
19	1	2	1	2	2	1	2	0	1	1	4	4	3	0	1	6	4	3	7	0	2	4
20	2	1	0	0	0	1	1	0	1	1	5	4	2	0	1	6	9	3	5	4	1	4
21	1	0	0	0	0	0	3	1	0	2	4	4	0	0	1	2	7	2	9	1	3	11
Max	2	0	2	1	0	1	1	0	0	3	3	3	5	0	0	0	7	4	6	1	4	8

For each printed pattern, width of the gel deposit was measured at the “Positions”. The measurements were then sorted from the lowest value to the highest value. Then the positions are ranked from the position who gave the lowest value to the position that gave the highest value. Finally, the number of times a position appears at each rank is reported on the table. As an example, the position number 1 has been the minimum value twelve times, conversely, the position 22 has been the maximum value eight times.

Conditional formatting was applied line by line, which means that within a line the cells of the table are colored in a gradient of green where the cell containing the minimum number is not colored, and the color green gets more and more intense as the number increases. As an example: in the first line (min), 12 is the highest number, therefore the cell containing the number 12 is colored with the most intense green. Whereas in the seventh line, 6 is the highest number, therefore each cell containing the number 6 are colored with the most intense green.

As presented in this table, the gel deposit tends to be thinner at the beginning of the print, and enlarges wider and wider until the end of the print. We can observe a cluster of intense green cell at the top left part of the table [position from 1 to 9- range form min to 11] and a cluster of green cells at the bottom right part of the table [position from 16 to 22, range from 16 to max].

SI-4- Hydrolysis of N-alkyl-D-galactonamide gel upon heating at 100°C – NMR data

N-alkyl-D-galactonamides solutions in D_2O are heated at 100°C for a time indicated in each spectrum. Signals of hydrolysis corresponding to the alkylammonium have been identified in the spectra and increased with the heating duration. Peak assignments are given in spectrum SI-4.2

SI-4.1- NMR spectrum of a suspension of N-octyl-D-galactonamide after 10 minutes at 100°C and 18h at room temperature

Particles of N-octyl-D-galactonamide powder are still in suspension. Concentration of GalC8 (total powder introduced): 5.5 µmol/mL in D_2O. DMSO as internal standard

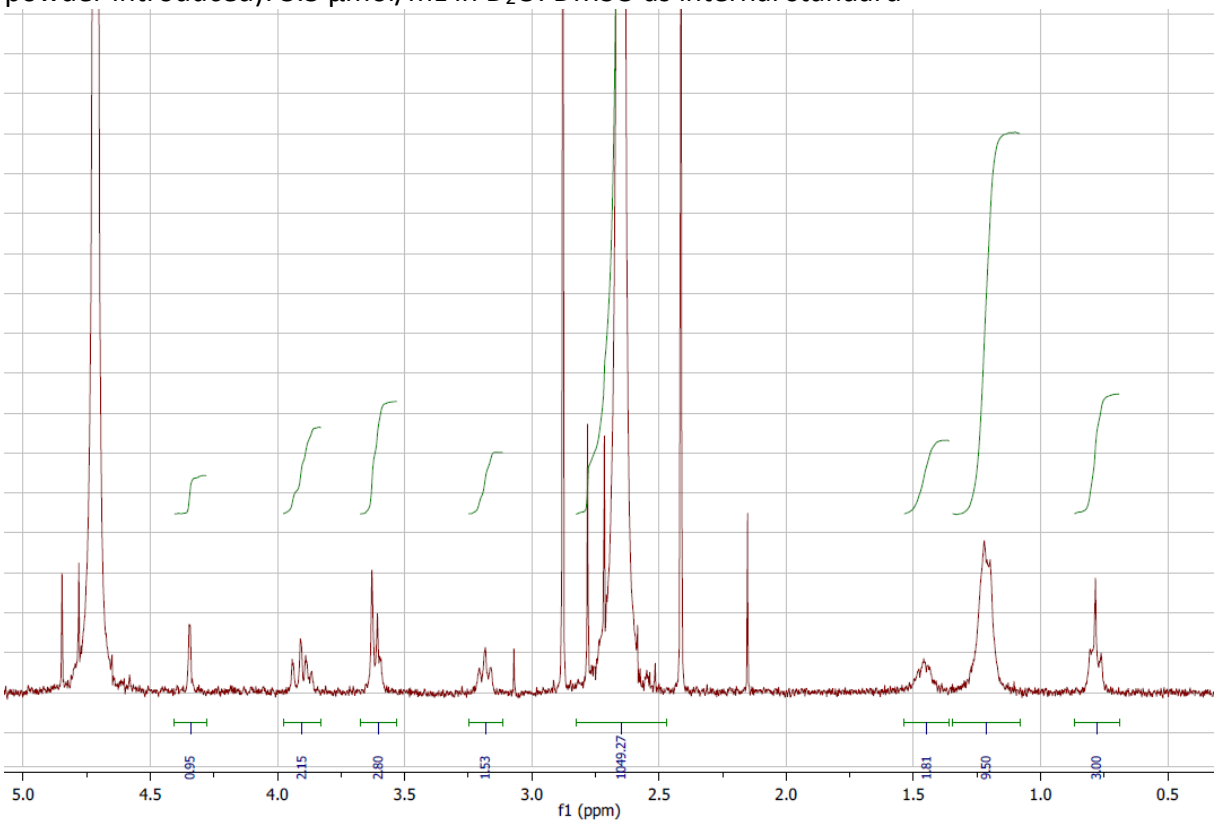

SI-4.2. NMR spectrum of a suspension of N-octyl-D-galactonamide after 1h at 100°C

Particles of N-octyl-D-galactonamide powder are still in suspension. Concentration of GalC8: 9.9 µmol/mL in D_2O. DMSO as internal standard

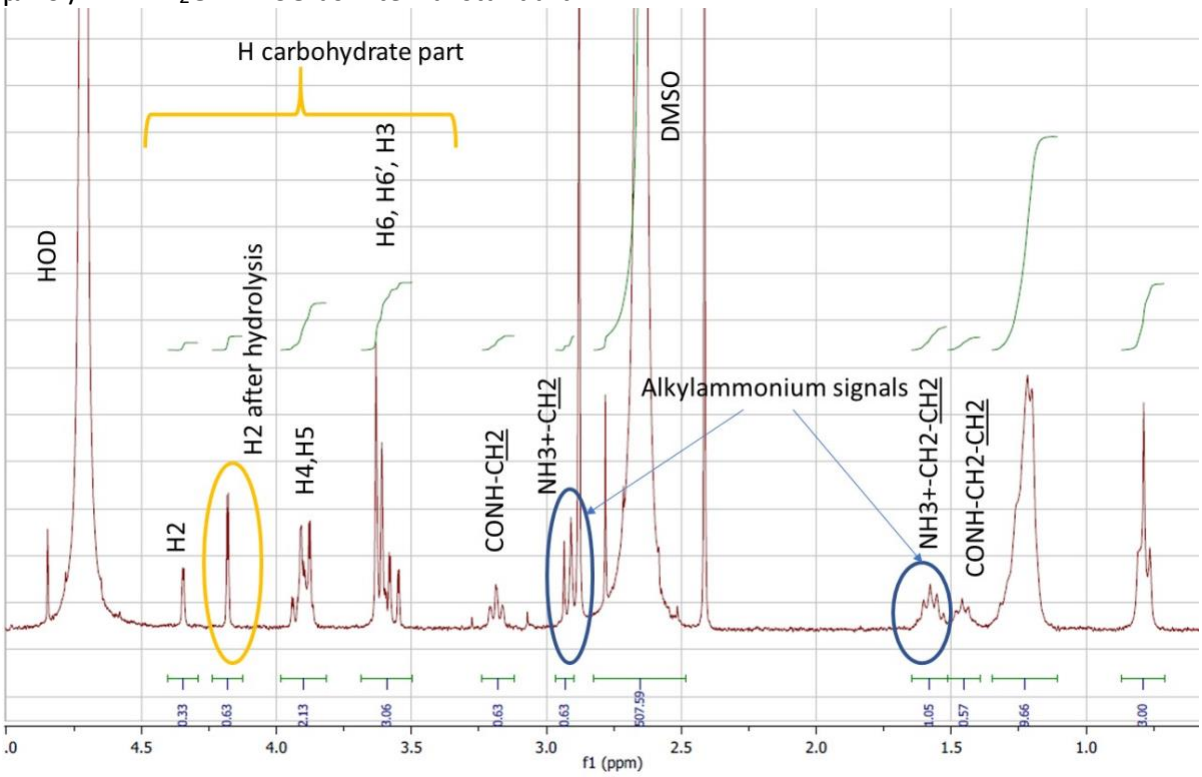

SI-4.3. MS spectrum of a suspension of N-octyl-D-galactonamide after 1h at 100°C (sample SI-4.2)

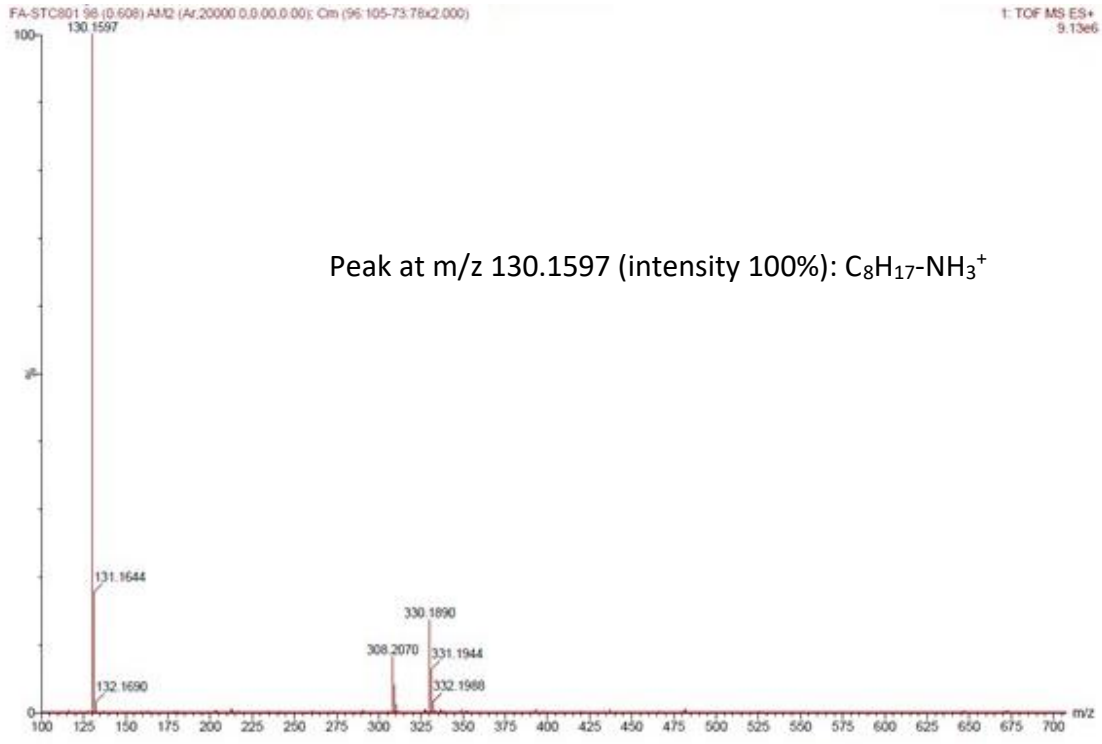

Peak at m/z 130.1597 (intensity 100%): C_8H_{17}-NH_3^+

Similar NMR and MS spectra have been obtained for N-nonyl-D-galactonamide in the same condition, with m/z = 144.1752 (intensity 100%), corresponding to C_9H_{19}-NH_3^+

SI-4.4. NMR spectrum of a suspension of N-heptyl-D-galactonamide after 10 min at 100°C and 48h at R.T.

Particles of N-heptyl-D-galactonamide powder are still in suspension. Concentration of GalC7 (total powder introduced): 2.35 µmol/mL in D_2O. DMSO as internal standard

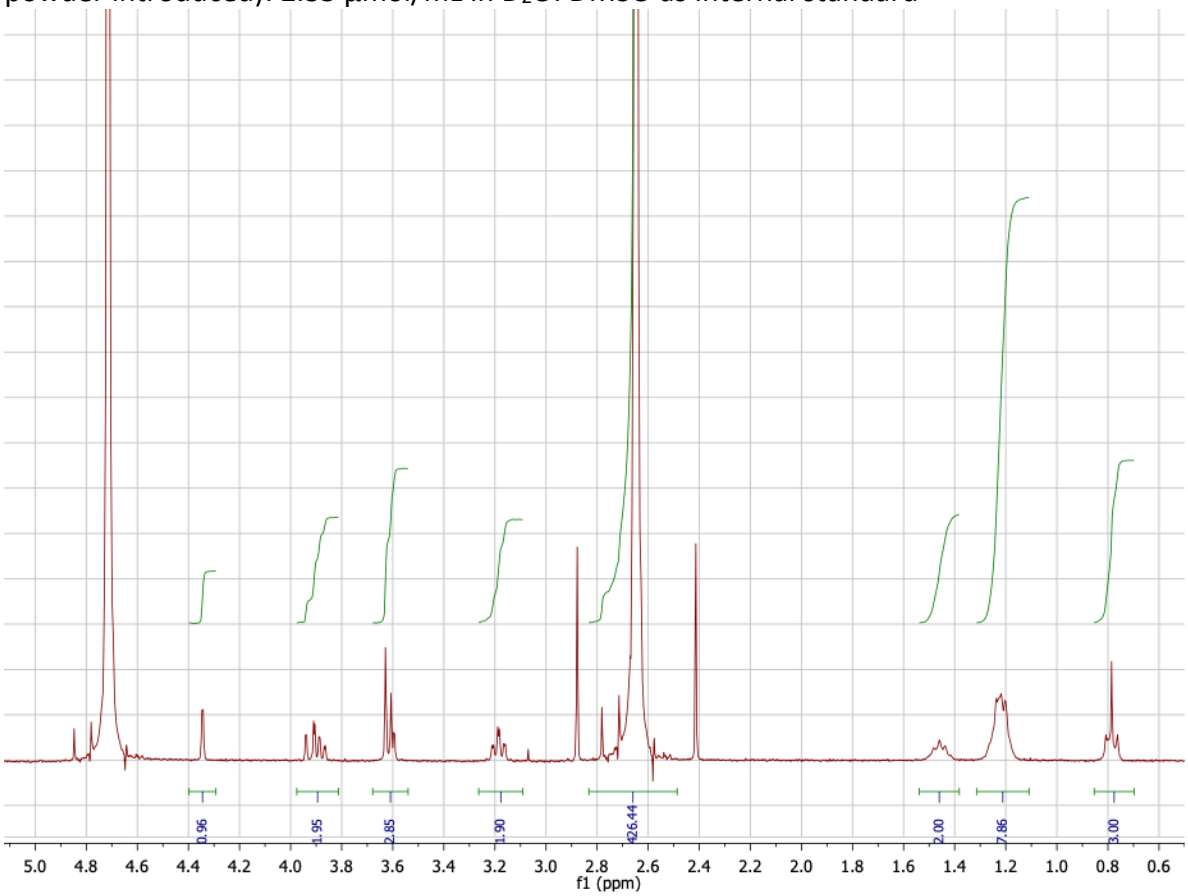

SI-4.5. NMR spectrum of a suspension of N-heptyl-D-galactonamide after 20 min at 100°C

A gel is formed in the whole volume of solution. Few particles of N-heptyl-D-galactonamide powder are still in suspension. Concentration of GalC7 (total powder introduced): 2.35 µmol/mL in D_2O. DMSO as internal standard

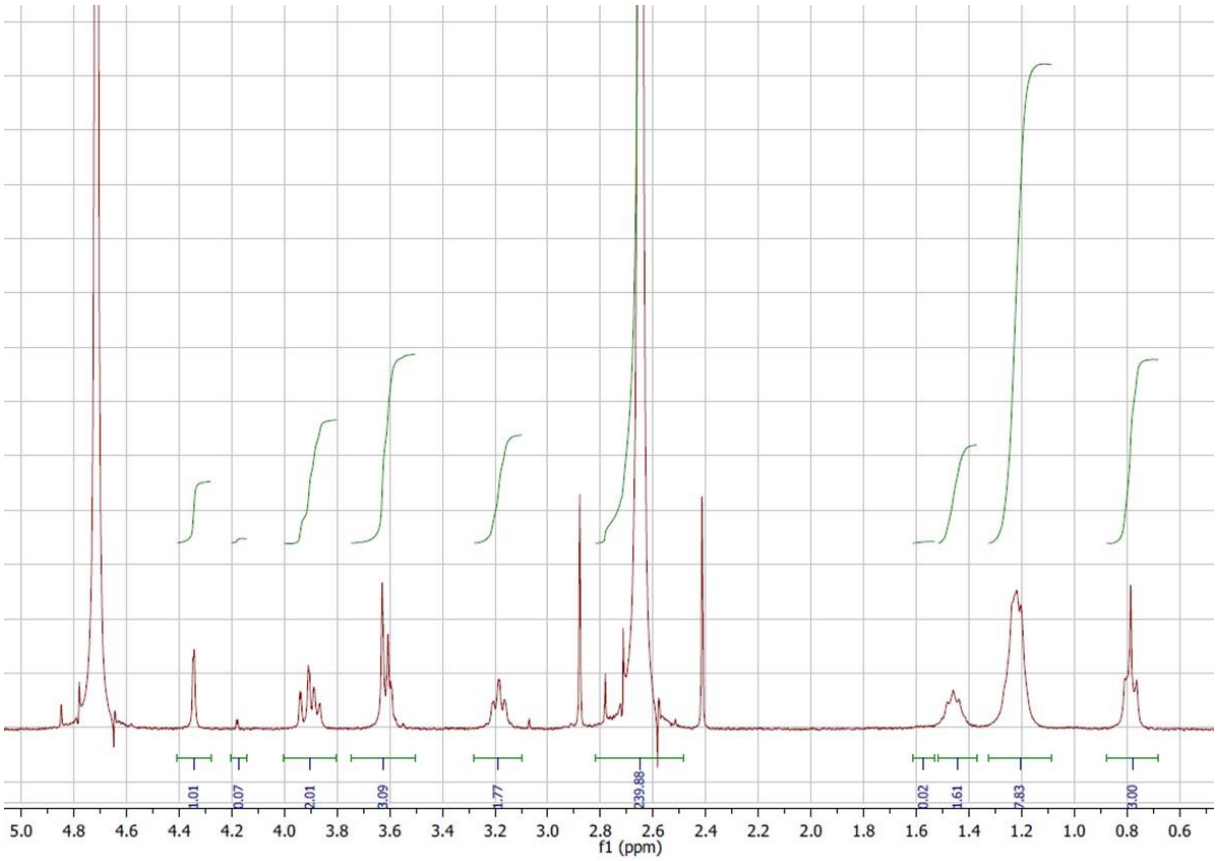

SI-5 Other examples of imbricated structures before and after dissolution of the sacrificial ink

Fig. SI-5.1: Superposition of 10 layers of GalC9 1% gel on 20 layers of GalC6 gel 5%. Pictures taken (a) just after the printing, (b) after 5 days.

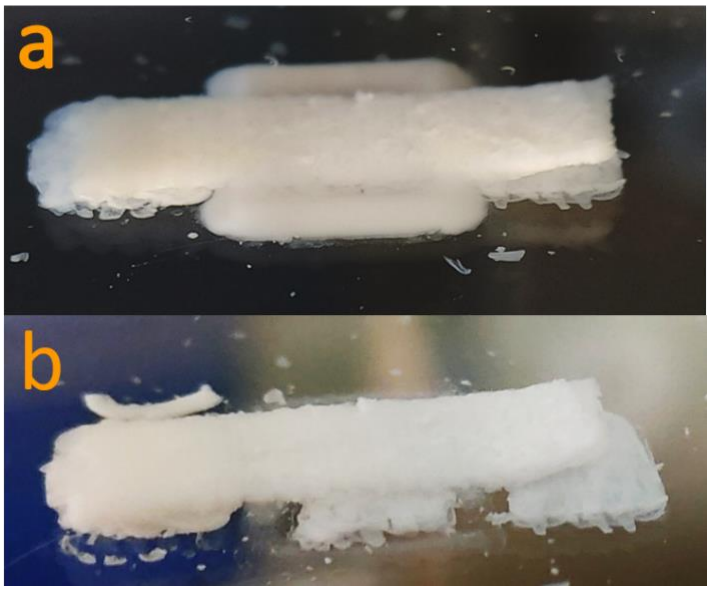

Fig. SI-5.2: Superposition of 10 layers of GalC9 1% gel on 10 layers of GalC7 gel 2.5%. Pictures taken (a) just after the printing, (b) after 7 days (c) after addition of 25mL of water and another 7 days

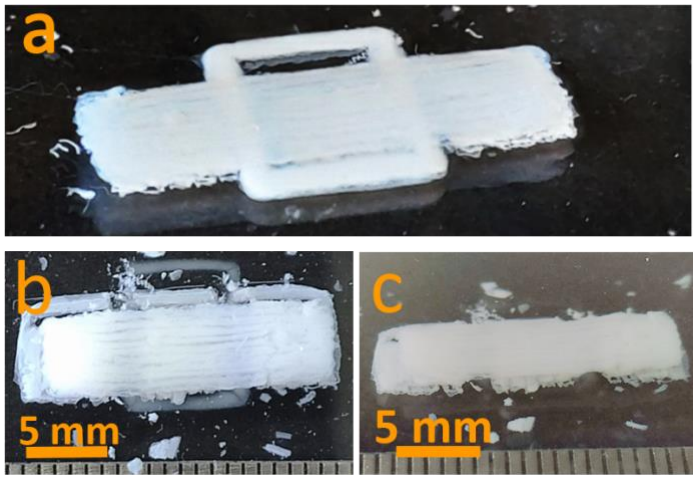

SI-6 – Supplementary images of cell culture assays

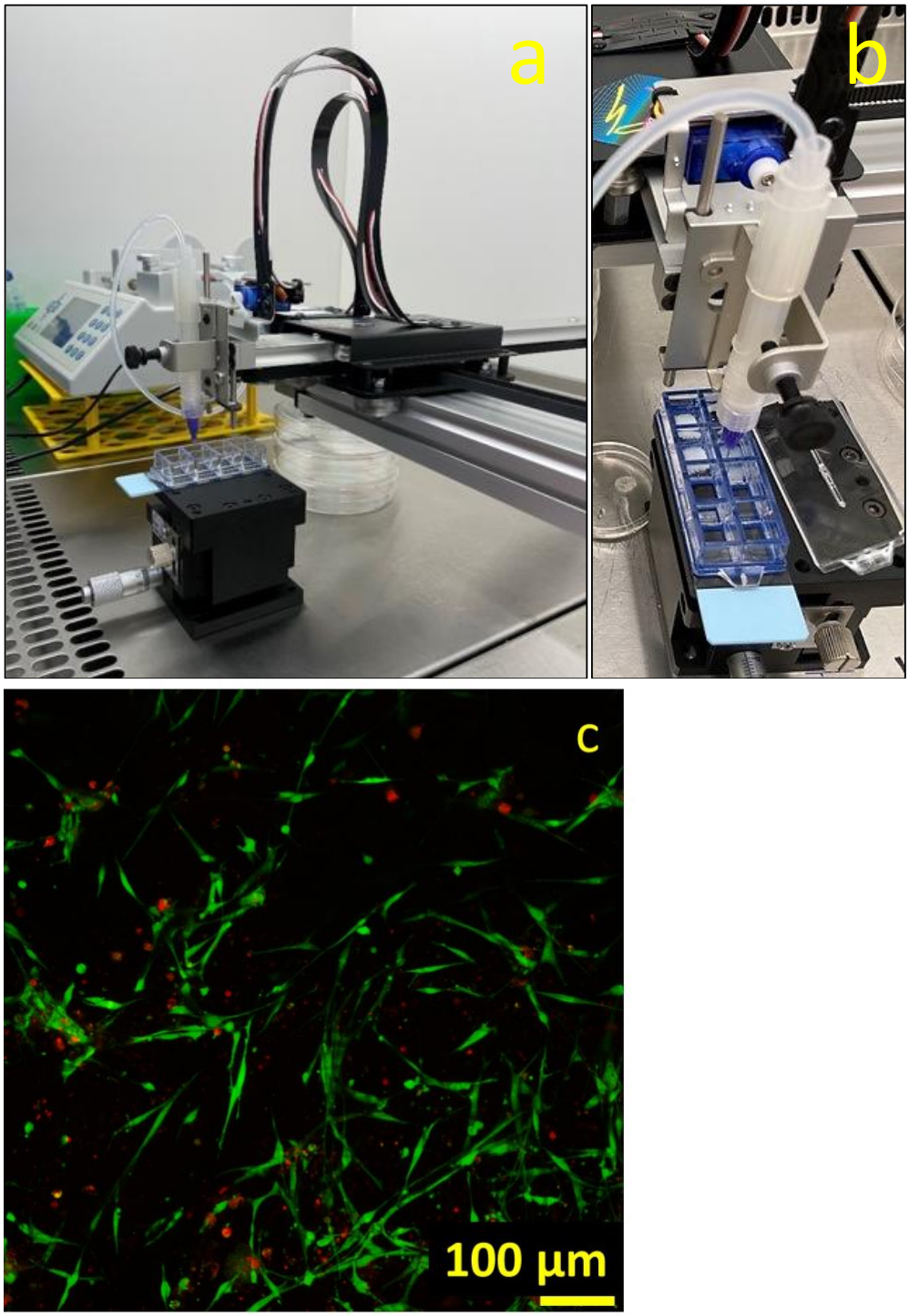

Fig. 8. (a,b) 3D printing equipment for cell culture assays (Axidraw, Fusion Syringe pump, manual Z micrometric platform); (c) Live-dead assays of mesenchymal stem cells after 7 days on a N-nonyl-D-galactonamide hydrogel prepared by cooling a hot solution.